

Optimal control of an optical quantum memory based on noble-gas spins

Or Katz,^{1,2,*} Roy Shaham,^{1,2,*} Eran Reches,¹ Alexey V. Gorshkov,³ and Ofer Firstenberg¹

¹*Department of Physics of Complex Systems, Weizmann Institute of Science, Rehovot 76100, Israel*

²*Rafael Ltd, IL-31021 Haifa, Israel*

³*Joint Quantum Institute and Joint Center for Quantum Information and Computer Science, NIST/University of Maryland, College Park, Maryland 20742, USA*

In Ref. [Katz *et al.*, arXiv:2007.08770 (2020)], we present a mechanism and optimal procedures for mapping the quantum state of photons onto an optically inaccessible macroscopic state of noble-gas spins, which functions as a quantum memory. Here we introduce and analyze a detailed model of the memory operation. We derive the equations of motion for storage and retrieval of non-classical light and design optimal control strategies. The detailed model accounts for quantum noise and for thermal atomic motion, including the effects of optical mode structure and imperfect anti-relaxation wall coating. We conclude with proposals of practical experimental configurations of the memory, with lifetimes ranging from seconds to hours.

I. INTRODUCTION

Optical quantum memories enable the storage and retrieval of an optical signal while preserving its quantum properties. In quantum information science, they can function as variable delay lines, leaving a quantum state unchanged during the memory operation [1]. Optical quantum memories are vital for applications such as quantum repeaters in long-distance quantum communication [2–5], conversion of heralded photons to on-demand single photons [6–8], synchronization of optical quantum computation [9], distribution of entanglement [10, 11], and metrology beyond the standard quantum limit [12–16].

Existing quantum memories are based on actual delay lines and cavities [1] or on a reversible mapping onto coherent excitations in matter [17]. The latter relies on strong light-matter coupling, known as the cooperativity, or the collective cooperativity in ensembles. The mapping process employs a variety of schemes, including electromagnetically induced transparency (EIT) [18–21], off-resonant Raman interaction [22–24], teleportation via the Faraday interaction [25–27], and a range of echo techniques [28, 29]. Solid media, such as defects in diamonds and rare-earth-doped crystals [30–32], as well as cold and warm atomic gases, primarily alkali-metal atoms [33–38], are utilized. The memory efficiency is determined by the cooperativity, while the storage duration (memory lifetime) is governed by the isolation of the matter excitation from the environment. Generally, high memory efficiencies are achieved with sub-millisecond memory lifetimes, whereas memories with longer lifetimes typically suffer from low efficiencies [39].

Rare isotopes of noble gases, such as ^3He , possess nonzero nuclear spins, which are isolated from the environment due to the enclosing, complete, electronic shells. These spins exhibit lifetimes exceeding hours at or above room temperature [40, 41] and are employed for medical lung imaging [42, 43], for precision magnetometers and NMR [44–47], for neutron spin filters [48], and for

searches of beyond-standard-model physics [49–52]. Unfortunately, these spins are optically inaccessible and are thus extremely hard to prepare, interface, and monitor. They are accessible, however, through collisions with other optically-active atoms, either metastable helium atoms via *strong* metastable-exchange collisions [40, 53] or alkali-metal atoms via *weak* spin-exchange collisions [40, 54, 55].

The first proposal to utilize noble-gas spins as a quantum memory was based on the former, with metastable helium population sustained by electric discharge [56]. Metastable exchange collisions rely on the strong electrostatic exchange interaction, leading to a complete transfer of the electronic configuration in a single collision (hence the terminology “strong” collision). The ground-state atom may be excited to the metastable state, and the metastable atom is then de-excited to the electronic ground-state, but both atoms maintain their nuclear states, and thus these collisions act to equilibrate the nuclear spin between the metastable and ground-state populations. A memory scheme relying on metastable exchange necessitates high collective optical cooperativity of the metastable population, which in turn requires either high-finesse cavities or higher helium densities (practically limited by Penning collisions), and the scheme has never been demonstrated.

Spin-exchange collisions between alkali and noble-gas atoms, on the other hand, involve the weak isotropic hyperfine interaction, where only a small fraction (10^{-4} – 10^{-6}) of the spin orientation is transferred in a single collision [54]. Numerous collisions can then accumulate to a collective, coherent evolution of the two spin ensembles, leading to an exchange of collective excitations that is free from excess thermalization and quantum noise [57]. Unlike with metastable helium, the alkali vapor density (highly sensitive to temperature) is independent of the noble-gas density (determined by pressure). It is therefore feasible to increase the alkali density and reach high optical cooperativity. At the same time, the coherent coupling between the collective alkali and collective

noble-gas spins can be made efficient and – by varying external magnetic fields – externally controllable. Utilization of the spin-exchange interaction to optically initialize and measure noble-gas spin systems has been considered [58]. The reversible mapping of optical signals, and non-classical states in particular, has never been studied.

In Ref. [59], we present the mechanism and the procedures for mapping the quantum state of photons onto the macroscopic spin state of noble gases via spin-exchange collisions. Here we extend the analysis and consider additional aspects of the alkali-mediated interface between photons and noble-gas spins. We derive the equations of motion of the system in a Bloch-Heisenberg-Langevin framework. The derivation includes the stochastic noise induced by thermalization, the effect of atomic thermal motion, nonuniform spatial profile of the optical fields, and possible spin relaxation at the cell walls. Subsequently, we describe the optimal control technique and identify optimal strategies for memory operation. We investigate feasible experimental conditions for realizing such memories, including various alkali-metal and noble-gas mixtures, and a range of temperatures, coatings, and gas pressures. This work can thus be used to design and realize viable quantum memories for nonclassical light employing macroscopic quantum states of noble-gas spins.

II. MODEL OF THE SYSTEM

A. System constituents

Consider an atomic enclosure of volume V containing N_a alkali-metal spins and N_b noble-gas spins, positioned inside an optical cavity as shown in Fig. 1. The alkali spins are initially polarized along the \hat{z} axis by optical pumping, and the noble-gas spins are hyper-polarized via spin-exchange optical pumping (SEOP) [55, 60]. In the presence of an optical quantum field, which serves as the signal, the total Hamiltonian of the system is given by

$$\tilde{\mathcal{H}} = \tilde{\mathcal{H}}_\varepsilon + \tilde{\mathcal{H}}_a + \tilde{\mathcal{H}}_b + \tilde{\mathcal{H}}_{a-\varepsilon} + \tilde{\mathcal{H}}_{a-b}. \quad (1)$$

Here $\tilde{\mathcal{H}}_\varepsilon$ is the Hamiltonian of the signal light field, $\tilde{\mathcal{H}}_a$ is the Hamiltonian of the alkali-metal spins, $\tilde{\mathcal{H}}_b$ is the Hamiltonian of the nuclear spins of the noble gas, $\tilde{\mathcal{H}}_{a-\varepsilon}$ is the atom-light dipole interaction, and $\tilde{\mathcal{H}}_{a-b}$ is the coherent spin-exchange interaction between the electronic spin of the alkali atoms and the nuclear spins of the noble-gas atoms [57].

Each polarized alkali-metal atom, labeled by a , is modeled as a three-level system in a Λ configuration, consisting of two ground-level states $|\tilde{\downarrow}\rangle_a$ and $|\tilde{\uparrow}\rangle_a$ and a single excited state $|\tilde{\rho}\rangle_a$, as shown in Fig. 1(b). The correspond-

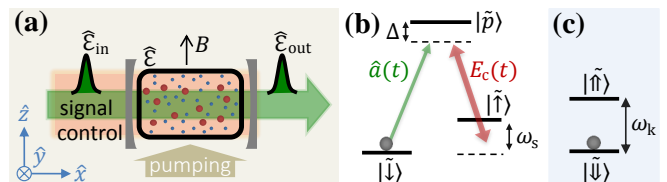


Figure 1. (a) A quantum memory system based on a mixture of noble-gas and alkali spins. The alkali-metal atoms (red) and noble-gas atoms (blue) interact with the quantum signal field $\hat{\mathcal{E}}$ in a cavity and with a classical control field. The atomic spins are initially polarized with an auxiliary pumping beam. The signal field in the cavity is coupled to the incoming field $\hat{\mathcal{E}}_{\text{in}}$, to be stored, and to the output field $\hat{\mathcal{E}}_{\text{out}}$, retrieved on demand after the memory time. (b) Energy levels of the modeled alkali atom in the lab frame. The Λ system consists of two stable ground-level states $|\tilde{\uparrow}\rangle$ and $|\tilde{\downarrow}\rangle$, coupled via an excited state $|\tilde{\rho}\rangle$ by the classical control field E_c and the quantum signal $\hat{a} = e^{-i\omega_\varepsilon t} \hat{\mathcal{E}}$. Initially, the state $|\tilde{\downarrow}\rangle$ is populated. (c) Energy levels of the modeled noble-gas atom in the lab frame. Initially, the state $|\tilde{\downarrow}\rangle$ is populated.

ing Hamiltonian is

$$\tilde{\mathcal{H}}_a = \hbar \sum_{a=1}^{N_a} (\omega_p |\tilde{\rho}\rangle_a \langle \tilde{\rho}|_a + \omega_s |\tilde{\uparrow}\rangle_a \langle \tilde{\uparrow}|_a), \quad (2)$$

where ω_p is the resonance frequency of the optical transition $|\tilde{\downarrow}\rangle - |\tilde{\rho}\rangle$, and ω_s is the frequency difference between $|\tilde{\downarrow}\rangle$ and $|\tilde{\uparrow}\rangle$. If the two spin states are in the same hyperfine manifold, then $\omega_s = g_s B$ corresponds to the Zeeman splitting, where $\mathbf{B} = B\hat{z}$ is the magnetic field, and $g_s = 2.8/[I] \times 2\pi \text{ MHz/G}$ is the gyromagnetic ratio of an alkali atom with nuclear spin I ($[I] \equiv 2I + 1$).

We consider noble-gas atoms with nuclear spin-1/2 (*e.g.*, ^3He and ^{129}Xe). Each noble-gas atom, labeled by b , consists of two spin levels $|\tilde{\downarrow}\rangle_b$ and $|\tilde{\uparrow}\rangle_b$, as shown in Fig. 1(c). The corresponding Hamiltonian is

$$\tilde{\mathcal{H}}_b = \hbar \sum_{b=1}^{N_b} \omega_k |\tilde{\uparrow}\rangle_b \langle \tilde{\uparrow}|_b, \quad (3)$$

with $\omega_k = g_k B$ being the frequency difference between the states $|\tilde{\uparrow}\rangle$ and $|\tilde{\downarrow}\rangle$ due to the Zeeman splitting of the noble-gas spins with gyromagnetic ratio g_k .

We shall adopt a cavity model for describing the quantum optical field [61]. We assume that the signal field resides in a single mode of a running-wave cavity, as described by the Hamiltonian

$$\tilde{\mathcal{H}}_\varepsilon = \hbar \omega_\varepsilon \hat{a}^\dagger \hat{a}. \quad (4)$$

Here \hat{a} is the bosonic annihilation operator of the electromagnetic field of the cavity mode with frequency ω_ε .

The atom-photon interaction Hamiltonian in the dipole approximation is given by

$$\tilde{\mathcal{H}}_{a-\varepsilon} = - \sum_{a=1}^{N_a} \hat{\mathbf{d}}_a \cdot \hat{\mathbf{E}}(\mathbf{r}_a, t), \quad (5)$$

where $\hat{\mathbf{d}}_a$ is the dipole operator of the alkali-metal atoms, and $\hat{\mathbf{E}}(\mathbf{r}_a, t)$ is the electric field at the location \mathbf{r}_a of that atom. In our model, the electric field is composed of a classical control field and a quantum signal. The control field, with frequency ω_c and amplitude $E_c f_c(\mathbf{r})$, couples to the $|\downarrow\rangle_a - |\tilde{\text{p}}\rangle_a$ transition, with dipole moment μ_c . The quantum signal field $\sqrt{\hbar\omega_\varepsilon/(2\epsilon_0)}f_\varepsilon(\mathbf{r})\hat{a}(t)$ couples to the $|\uparrow\rangle_a - |\tilde{\text{p}}\rangle_a$ transition, with dipole moment μ_ε . We thus obtain

$$\begin{aligned} \tilde{\mathcal{H}}_{a-\varepsilon} = & - \sum_{a=1}^{N_a} f_c(\mathbf{r}_a)\mu_c E_c(t)e^{-i\omega_c t}|\tilde{\uparrow}\rangle_a\langle\tilde{\text{p}}|_a + \text{h.c.} \\ & - \sum_{a=1}^{N_a} f_\varepsilon(\mathbf{r}_a)\mu_\varepsilon\sqrt{\frac{\hbar\omega_\varepsilon}{2\epsilon_0}}\hat{a}(t)|\tilde{\downarrow}\rangle_a\langle\tilde{\text{p}}|_a + \text{h.c.} \end{aligned} \quad (6)$$

The spatial mode functions $f_c(\mathbf{r})$ and $f_\varepsilon(\mathbf{r})$ satisfy the Helmholtz equation

$$(\nabla^2 + k_i^2)f_i(\mathbf{r}) = 0, \quad (7)$$

where $i \in \{\varepsilon, c\}$, with the boundary conditions determined by the cavity: $f_c(\mathbf{r})$ is the solution with an eigenvalue $k_c = \omega_c/c$, and $f_\varepsilon(\mathbf{r})$ is the solution with an eigenvalue $k_\varepsilon = \omega_\varepsilon/c$, where c denotes the speed of light. The Rabi frequency of the classical field within the cavity is given by $\Omega(\mathbf{r}, t) = \sqrt{V_{\text{cav}}}f_c(\mathbf{r})\Omega(t)$, where $\Omega(t) = \mu_c E_c(t)/(\hbar\sqrt{V_{\text{cav}}})$. Similarly, $g(\mathbf{r}) = \sqrt{V_{\text{cav}}}g f_\varepsilon(\mathbf{r})$ is the one-photon Rabi frequency for the quantized-field mode, where [61]

$$g = \mu_\varepsilon\sqrt{\omega_\varepsilon/(2\epsilon_0\hbar V_{\text{cav}})}. \quad (8)$$

Before discussing the spin-exchange interaction $\tilde{\mathcal{H}}_{a-b}$, we transform the above Hamiltonians into a rotating frame. The transformation is given by

$$U_a = e^{i\omega_\varepsilon t}|\text{p}\rangle_a\langle\tilde{\text{p}}|_a + e^{i(\omega_\varepsilon - \omega_c)t}|\uparrow\rangle_a\langle\tilde{\uparrow}|_a + |\downarrow\rangle_a\langle\tilde{\downarrow}|_a \quad (9)$$

for any alkali spin a , and by

$$U_b = e^{i(\omega_\varepsilon - \omega_c)t}|\uparrow\rangle_b\langle\tilde{\uparrow}|_b + |\downarrow\rangle_b\langle\tilde{\downarrow}|_b \quad (10)$$

for any noble-gas spin b . We also use the transformation $U_\varepsilon = e^{i\frac{t}{\hbar}\mathcal{H}_\varepsilon}$ for the signal field and define the slowly varying quantum field operator $\hat{\mathcal{E}}(t) = e^{i\omega_\varepsilon t}\hat{a}(t)$, which describes the envelope of the quantum field within the cavity. We further define the slowly-varying continuous atomic operators

$$\hat{\sigma}_{\mu\nu}(\mathbf{r}, t) = \sum_{a=1}^{N_a} |\mu\rangle_a\langle\nu|_a\delta(\mathbf{r} - \mathbf{r}_a), \quad (11)$$

which describe the collective state of the alkali ensemble with $\mu, \nu \in \{\downarrow, \uparrow, \text{p}\}$, and

$$\hat{\sigma}_{\mu\nu}(\mathbf{r}, t) = \sum_{b=1}^{N_b} |\mu\rangle_b\langle\nu|_b\delta(\mathbf{r} - \mathbf{r}_b), \quad (12)$$

which describe the collective state of the noble-gas ensemble with $\mu, \nu \in \{\downarrow, \uparrow\}$. In the rotating frame, we get

$$\begin{aligned} \mathcal{H} - \mathcal{H}_{a-b} = & \hbar \int_V d^3\mathbf{r} \Delta\hat{\sigma}_{\text{pp}} + \tilde{\delta}_s\hat{\sigma}_{\uparrow\uparrow} + \tilde{\delta}_k\hat{\sigma}_{\uparrow\uparrow} \\ & - \left[\Omega(\mathbf{r}, t)\hat{\sigma}_{\text{p}\uparrow} + g(\mathbf{r})\hat{\mathcal{E}}(t)\hat{\sigma}_{\text{p}\downarrow} + \text{h.c.} \right], \end{aligned} \quad (13)$$

where $\Delta = \omega_p - \omega_\varepsilon$ is the one-photon detuning from the atomic optical transition, and $\tilde{\delta}_s = \omega_s + \omega_c - \omega_\varepsilon$ and $\tilde{\delta}_k = \omega_k + \omega_c - \omega_\varepsilon$ are the two-photon detunings from the spin resonances of the two species (absent the shifts induced by the spin-exchange interaction).

B. Spin-exchange coupling

The two spin gases experience random, weak, spin-exchange collisions. For polarized gases, the leading term in the dynamics is described by the coherent interaction Hamiltonian [57]

$$\tilde{\mathcal{H}}_{a-b} = \hbar\zeta \int d^3\mathbf{r}_1 \int d^3\mathbf{r}_2 \delta(\mathbf{r}_1 - \mathbf{r}_2) \hat{\mathbf{f}}(\mathbf{r}_1, t) \cdot \hat{\mathbf{k}}(\mathbf{r}_2, t), \quad (14)$$

where $\hat{\mathbf{f}}(\mathbf{r}, t) \equiv \sum_a \hat{\mathbf{f}}_a(t)\delta(\mathbf{r} - \mathbf{r}_a(t))$ and $\hat{\mathbf{k}}(\mathbf{r}, t) \equiv \sum_b \hat{\mathbf{k}}_b(t)\delta(\mathbf{r} - \mathbf{r}_b(t))$ denote the continuous spin operators of alkali and noble-gas spins, respectively. $\zeta\delta(\mathbf{r}_1 - \mathbf{r}_2)$ is the local average interaction strength of an alkali and noble-gas atom pair, where the microscopic interaction strength constant $\zeta = \langle\phi\sigma v\rangle_c/[I]$ is given by ensemble averaging over all realizations of the collisional parameters, given the velocity v , the hard-sphere cross-section σ , and the accumulated phase ϕ during a single collision instance.

The ground level of actual alkali-metal atoms consists of multiple spin levels. We choose $|\downarrow\rangle_a$ to be the maximally-polarized spin state (with the projection $I+1/2$ along the quantization axis) and choose $|\uparrow\rangle_a$ to be the adjacent state (with projection $I-1/2$); both states are in the hyperfine manifold $F = I + 1/2$. With this choice and for fully polarized ensembles, it is a good approximation to replace the total spin operator $\hat{\mathbf{f}}$ by its projection on the two-state subsystem $\hat{\mathbf{f}} \approx \hat{P}\hat{\mathbf{f}}\hat{P}$, where $\hat{P} = \sum_a (|\uparrow\rangle_a\langle\uparrow|_a + |\downarrow\rangle_a\langle\downarrow|_a)$. We then obtain in the rotating frame

$$\begin{aligned} \hat{\mathbf{f}}(\mathbf{r}, t) \approx & \frac{[I]}{2}(\hat{\sigma}_{\downarrow\downarrow} + q_I\hat{\sigma}_{\uparrow\uparrow})\mathbf{e}_z \\ & + \sqrt{\frac{[I]}{2}}(e^{i(\omega_c - \omega_\varepsilon)t}\hat{\sigma}_{\downarrow\uparrow}\mathbf{e}_- + \text{h.c.}), \end{aligned} \quad (15)$$

where $\mathbf{e}_\pm = (\mathbf{e}_x \pm i\mathbf{e}_y)/\sqrt{2}$ and $q_I = ([I] - 2)/[I]$.

The collective noble-gas spin operator appearing in Eq. (14) is given in the rotating frame by

$$\begin{aligned} \hat{\mathbf{k}}(\mathbf{r}, t) = & \frac{1}{2}(\hat{\sigma}_{\downarrow\downarrow} - \hat{\sigma}_{\uparrow\uparrow})\mathbf{e}_z \\ & + \sqrt{\frac{1}{2}}(e^{i(\omega_c - \omega_\varepsilon)t}\hat{\sigma}_{\downarrow\uparrow}\mathbf{e}_- + \text{h.c.}). \end{aligned} \quad (16)$$

We thus arrive at the spin-exchange Hamiltonian

$$\mathcal{H}_{a-b} = \hbar \int_V d^3\mathbf{r} \left[\mathcal{H}_s + \zeta \sqrt{|I|} (\hat{\sigma}_{\downarrow\uparrow} \hat{\sigma}_{\uparrow\downarrow} + \text{h.c.}) / 2 \right], \quad (17)$$

where the first term

$$\mathcal{H}_s(\mathbf{r}, t) = \zeta [I] (\hat{\sigma}_{\downarrow\downarrow} + q_I \hat{\sigma}_{\uparrow\uparrow}) (\hat{\sigma}_{\downarrow\downarrow} - \hat{\sigma}_{\uparrow\uparrow}) / 4 \quad (18)$$

describes an additional energy shift, which becomes prominent for polarized ensembles. The second term in Eq. (17) manifests the conservative exchange of spin between the two gases.

C. Dissipation and atomic motion

The system Hamiltonian \mathcal{H} given by Eqs. (13) and (17) constitutes the unitary evolution of the system. The system is however coupled to the environment: the cavity field decays at a rate κ through the output port; the optical coherence between $|\downarrow\rangle$ and $|p\rangle$ decays at a rate $\gamma_{\downarrow p}$, coming from the decay of state $|p\rangle$ to the ground state (by emitting photons or by non-radiative channels via inelastic collisions) or from collisional dephasing; and the alkali-spin and noble-gas-spin coherences relax at rates $\gamma_{\downarrow\uparrow}$ and $\gamma_{\uparrow\downarrow}$, respectively, by various spin thermalization channels. In addition, the atoms are moving, and their thermal motion is rendered diffusive by the dense noble gas acting as a buffer [62]. We denote by D_a and D_b the spatial diffusion coefficients of the alkali and noble-gas atoms, respectively.

The overall dynamics can be described using the Heisenberg-Bloch-Langevin formalism of open quantum systems [17, 61, 63]. The atomic dynamics, in terms of the continuous quantum operators $\hat{\sigma}_{\mu\nu}(\mathbf{r}, t)$ in the Heisenberg picture, is given by the stochastic differential equations

$$\partial_t \hat{\sigma}_{\mu\nu} = \frac{i}{\hbar} [\mathcal{H}, \hat{\sigma}_{\mu\nu}] + (D_{a/b} \nabla^2 - \gamma_{\mu\nu}) \hat{\sigma}_{\mu\nu} + \hat{f}_{\mu\nu}. \quad (19)$$

The first term describes coherent evolution by the system Hamiltonian \mathcal{H} . The second term describes the decay of the system both due to the spatial diffusion and due to its coupling to the environment at a rate $\gamma_{\mu\nu}$. The third term describes the stochastic evolution through the input noise operators $\hat{f}_{\mu\nu}$, which depend on the thermal spin-state of the reservoir [64]. The explicit form of these equations is given in Eqs. (A1)-(A3).

D. Collective excitations of polarized ensembles

At this point, we focus on the regime of highly polarized spin ensembles, where Eqs. (13), (17), and (19) can be further simplified by using the Holstein-Primakoff transformation [17, 65]. This transformation replaces

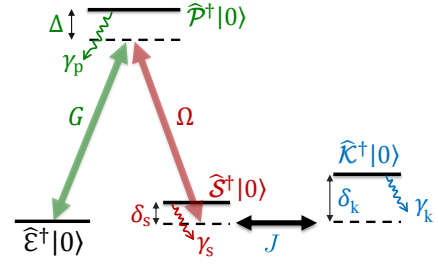


Figure 2. Couplings between the collective states for a single input photon. A single photon $\hat{\mathcal{E}}^\dagger|0\rangle$ in the cavity is transferred to the collective noble-gas spin excitation $\hat{\mathcal{K}}^\dagger|0\rangle$, which acts as the quantum memory, via intermediate excitations of the alkali collective excited-state $\hat{\mathcal{P}}^\dagger|0\rangle$ and ground-state $\hat{\mathcal{S}}^\dagger|0\rangle$ spins. The coupling is controlled by varying the strength of the control field $\Omega(t)$ and the detunings $\delta_s(t)$ and $\delta_k(t)$. The exchange coupling rate J and the decay rates γ_p , γ_s , and γ_k are constant. The state $|0\rangle$ corresponds to the maximally polarized spin state, and $\hat{\mathcal{P}}$, $\hat{\mathcal{S}}$, and $\hat{\mathcal{K}}$ are bosonic field operators.

the collective spin ladder operators with bosonic creation and annihilation operators. Let p_a and p_b denote the polarization degree of the alkali and noble-gas spin ensembles, respectively. For polarized spin ensembles ($p_a, p_b \approx 1$), the operators $\sigma_{\downarrow\downarrow} \approx p_a n_a$ and $\hat{\sigma}_{\downarrow\downarrow} \approx p_b n_b$ act as classical magnetic moments, where n_a and n_b are the alkali and noble-gas densities. The collective spin excitations, which remain quantum, can now be described by the operators $\hat{\mathcal{P}}(\mathbf{r}, t) = \hat{\sigma}_{\downarrow p}(\mathbf{r}, t) / \sqrt{p_a n_a}$, $\hat{\mathcal{S}}(\mathbf{r}, t) = \hat{\sigma}_{\downarrow\uparrow}(\mathbf{r}, t) / \sqrt{p_a n_a}$, and $\hat{\mathcal{K}}(\mathbf{r}, t) = \hat{\sigma}_{\downarrow\uparrow}(\mathbf{r}, t) / \sqrt{p_b n_b}$. These operators satisfy the bosonic commutation relations $[\hat{\mathcal{P}}(\mathbf{r}), \hat{\mathcal{P}}^\dagger(\mathbf{r}')] = [\hat{\mathcal{S}}(\mathbf{r}), \hat{\mathcal{S}}^\dagger(\mathbf{r}')] = [\hat{\mathcal{K}}(\mathbf{r}), \hat{\mathcal{K}}^\dagger(\mathbf{r}')] = \delta(\mathbf{r} - \mathbf{r}')$. Figure 2 reformulates the level structure of the system using these operators, for the case of a single excitation.

The equations of motion for the spin annihilation operators [see Eqs. (A5)-(A7)] are then given by

$$\partial_t \hat{\mathcal{P}}(\mathbf{r}, t) = -(\gamma_p + i\Delta) \hat{\mathcal{P}}(\mathbf{r}, t) + i\Omega(\mathbf{r}, t) \hat{\mathcal{S}}(\mathbf{r}, t) + iG(\mathbf{r}) \hat{\mathcal{E}}(t) + \hat{f}_{\mathcal{P}}(\mathbf{r}, t), \quad (20)$$

$$\partial_t \hat{\mathcal{S}}(\mathbf{r}, t) = -(\gamma_s + i\delta_s - D_a \nabla^2) \hat{\mathcal{S}}(\mathbf{r}, t) + i\Omega^*(\mathbf{r}, t) \hat{\mathcal{P}}(\mathbf{r}, t) - iJ \hat{\mathcal{K}}(\mathbf{r}, t) + \hat{f}_{\mathcal{S}}(\mathbf{r}, t), \quad (21)$$

$$\partial_t \hat{\mathcal{K}}(\mathbf{r}, t) = -(\gamma_k + i\delta_k - D_b \nabla^2) \hat{\mathcal{K}}(\mathbf{r}, t) - iJ \hat{\mathcal{S}}(\mathbf{r}, t) + \hat{f}_{\mathcal{K}}(\mathbf{r}, t). \quad (22)$$

Here δ_s and δ_k are the two-photon detunings associated with the collective spin operators of the alkali and noble gas, respectively. They correspond to the previously-defined $\tilde{\delta}_s$ and $\tilde{\delta}_k$, but also include the collisional shifts due to the spin-exchange collisions (see Appendix A). $G(\mathbf{r}) = \sqrt{p_a n_a} g(\mathbf{r})$ denotes the collective interaction rate of the optical dipole with the optical field in the cavity, and $J = \zeta \sqrt{|I| p_a p_b n_a n_b} / 4$ denotes the collective exchange rate of the two polarized spin ensembles, a con-

sequence of multiple weak spin-exchange collisions [57]. The stochastic properties of the quantum noise terms $\hat{f}_{\mathcal{P}}(\mathbf{r}, t)$, $\hat{f}_{\mathcal{S}}(\mathbf{r}, t)$ and $\hat{f}_{\mathcal{K}}(\mathbf{r}, t)$ are detailed in Appendix B.

Equations (20)-(22) manifest the collective enhancement of the various couplings to the collective excitations. The atom-photon interaction rate $g(\mathbf{r})$ is multiplied by the large factor $\sqrt{n_a}$, as expected for the coherent absorption and emission of a photon by multiple atoms, resulting with the enhanced collective rate $G(\mathbf{r})$. The microscopic coherent spin-exchange rate ζ is multiplied by $\sqrt{n_a n_b}$, corresponding to a unitary precession of the collective spin of one gas around the other at the enhanced rate J .

E. Dynamics of the light field

The dynamics of the slowly-varying quantum light field in the cavity $\hat{\mathcal{E}}(t)$ is described by the Heisenberg-Langevin equation

$$\begin{aligned} \partial_t \hat{\mathcal{E}} &= -\kappa \hat{\mathcal{E}} + \sqrt{2\kappa} \hat{\mathcal{E}}_{\text{in}} + \frac{i}{\hbar} [\mathcal{H}, \hat{\mathcal{E}}] \\ &= -\kappa \hat{\mathcal{E}} + \sqrt{2\kappa} \hat{\mathcal{E}}_{\text{in}} + i \int_V G^*(\mathbf{r}) \hat{\mathcal{P}}(\mathbf{r}, t) d^3\mathbf{r}. \end{aligned} \quad (23)$$

Here the cavity field decays at a rate κ and is driven by the field $\hat{\mathcal{E}}_{\text{in}}(t)$ at the cavity input port. The third term in Eq. (23) describes the collective absorption and emission of the field by the dipole coherence $\hat{\mathcal{P}}$. We implicitly assume that the cavity has no internal losses. The field $\hat{\mathcal{E}}_{\text{out}}(t)$ at the cavity output port is obtained from the general input-output relation [61]

$$\hat{\mathcal{E}}_{\text{out}} = \sqrt{2\kappa} \hat{\mathcal{E}} - \hat{\mathcal{E}}_{\text{in}}. \quad (24)$$

The commutation relations $[\hat{\mathcal{E}}_{\text{in}}(t), \hat{\mathcal{E}}_{\text{in}}^\dagger(t')] = [\hat{\mathcal{E}}_{\text{out}}(t), \hat{\mathcal{E}}_{\text{out}}^\dagger(t')] = \delta(t-t')$ hold. In the fast-cavity regime ($\kappa \gg G$, also known as a 'bad' cavity), the input-output relation simplifies to

$$\hat{\mathcal{E}}_{\text{out}} = \hat{\mathcal{E}}_{\text{in}} + i \sqrt{\frac{2}{\kappa}} \int_V G^*(\mathbf{r}) \hat{\mathcal{P}}(\mathbf{r}, t) d^3\mathbf{r}. \quad (25)$$

We adopt this approximation in our analysis, thus limiting the results to the fast-cavity regime. Notably, the operation of an optical quantum memory in this regime resembles the operation in free space [66].

To further simplify the analysis, we limit the bandwidth of the incoming light pulse to

$$T^{-1} \ll C\gamma_p, \quad (26)$$

where T is the pulse duration. The cooperativity parameter of the cavity is given by

$$C = \frac{|G|^2}{\gamma_p \kappa}, \quad (27)$$

characterizing the collective atom-photon interaction strength with respect to the decay rates, where $G = \sqrt{p_a n_a} g$ and g is given in Eq. (8). Under the assumptions of fast cavity and limited pulse bandwidth, $\hat{\mathcal{P}}$ adiabatically follows both the light field $\hat{\mathcal{E}}$ and the collective alkali-spin operators $\hat{\mathcal{S}}$, satisfying

$$\hat{\mathcal{P}}(\mathbf{r}, t) = i \frac{\Omega(\mathbf{r}, t) \hat{\mathcal{S}}(\mathbf{r}, t) + G(\mathbf{r}) \hat{\mathcal{E}}(t) - i \hat{f}_{\mathcal{P}}(\mathbf{r}, t)}{\gamma_p + i\Delta}. \quad (28)$$

III. SPATIAL MODES OF ATOMIC OPERATORS

Up until this point, we described the dynamics of the atomic spins using local continuous operators. Indeed, Eqs. (21), (22), and (28) support the storage of photons in multiple spatial modes [62]. The signal light field, however, was assumed to reside in the specific spatial mode $f_\varepsilon(\mathbf{r})$ of the cavity, with the input signal field matching this mode. Therefore, the signal excites an atomic superposition with a particular spatial amplitude pattern [via the term $\propto G(\mathbf{r}) \hat{\mathcal{E}}(t)$ in Eq. (28)], and subsequently this specific superposition coherently emits light to the output port [Eq. (25)]. In this section, we present the simplified equations of motion for a single uniform mode of the atomic operators. The general multi-mode evolution, governed by the nonlocal action of the diffusion operator, is presented in Appendix C and numerically calculated in Appendix D.

In the single-mode representation, the output field of the cavity is given by [compare to Eq. (25)]

$$\hat{\mathcal{E}}_{\text{out}}(t) = \hat{\mathcal{E}}_{\text{in}}(t) + i \sqrt{2C\gamma_p} \hat{\mathcal{P}}(t), \quad (29)$$

where the atomic optical dipole is [compare to Eq. (28)]

$$\hat{\mathcal{P}}(t) = \frac{i\Omega(t) \hat{\mathcal{S}}(t) + i \sqrt{2\gamma_p C} \hat{\mathcal{E}}_{\text{in}}(t) + \hat{f}_{\mathcal{P}}(t)}{\gamma_p (1+C) + i\Delta}. \quad (30)$$

The dynamics of the uniform mode $\hat{\mathcal{S}}$ of the alkali spin is given by

$$\partial_t \hat{\mathcal{S}} = -(\gamma_s + \Gamma_\Omega + i\delta_s) \hat{\mathcal{S}} - iJ\hat{\mathcal{K}} - Q\Omega^* \hat{\mathcal{E}}_{\text{in}} + \hat{F}_S \quad (31)$$

where the complex-valued optical coupling rate is

$$\Gamma_\Omega(t) \equiv \frac{|\Omega(t)|^2}{\gamma_p (1+C) + i\Delta}, \quad (32)$$

and we define

$$Q = \frac{\sqrt{2C\gamma_p}}{\gamma_p (1+C) + i\Delta}. \quad (33)$$

We identify $\gamma_\Omega \equiv \text{re}(\Gamma_\Omega)$ as the stimulated (power-broadened) optical coupling rate to the alkali spins, and $\text{im}(\Gamma_\Omega)$ as the light shift due to the control field. The

noise operator of the alkali spins is given by $\hat{F}_S = \hat{f}_S + iQ\Omega^* \hat{f}_P / \sqrt{2C\gamma_P}$, including the excess noise due to scattering of the control photons.

The uniform mode of the alkali spins has a large overlap with the long-lived uniform mode of the noble-gas spins, which is unaffected by diffusion [63] and therefore chosen as the quantum memory. The dynamics of the uniform mode $\hat{\mathcal{K}}$ of the noble-gas spin is given by

$$\partial_t \hat{\mathcal{K}} = -(\gamma_k + i\delta_k) \hat{\mathcal{K}} - iJ\hat{S} + \hat{f}_K. \quad (34)$$

The noise operators \hat{f}_P , \hat{f}_S , and \hat{f}_K are defined in Appendix C.

IV. MEMORY EFFICIENCY

Following Refs. [61, 67], we write the total efficiency of the quantum memory

$$\eta_{\text{tot}} = \eta_{\text{in}} \eta_{\text{dark}} \eta_{\text{out}} \quad (35)$$

in terms of the efficiency η_{in} of the storage process, the efficiency η_{out} of the retrieval process, and the efficiency (preservation of noble-gas spin coherence) in the dark

$$\eta_{\text{dark}} = \exp(-2\gamma_k \tau), \quad (36)$$

where τ is the memory (dark) time. The total efficiency η_{tot} sets a limit on other figures of merit, such as the memory fidelity [61] or preservation of squeezing [68–70].

As we will show and as could be expected, signal photons can be stored and retrieved with an efficiency approaching $\eta_{\text{in}} = \eta_{\text{out}} = C/(C+1)$ when their duration T is long enough, provided that $\gamma_k T \ll 1$. In this low-bandwidth limit, $\hat{\mathcal{P}}$ and \hat{S} are adiabatically eliminated, and the efficiency is only limited by the finite cooperativity of the cavity. However for practical operation of the memory, short signal pulses and correspondingly high memory bandwidth are desirable. The ideal adiabatic elimination then does not hold, and different optimal solutions arise. In the following sections, we analyze optimal strategies for storing incoming signals with finite typical duration T and for retrieving signals with the same typical duration.

A. Storage efficiency

The storage process starts with the arrival of the pulse and ends at $t = T'$. During this process, the input field of typical duration $T \leq T'$ is mapped onto the long-lived, collective, noble-gas spin $\hat{\mathcal{E}}_{\text{in}} \rightarrow \hat{\mathcal{K}}(T')$. We denote $\langle \hat{\mathcal{O}}^\dagger \hat{\mathcal{O}} \rangle_t = \langle \hat{\mathcal{O}}^\dagger(t) \hat{\mathcal{O}}(t) \rangle$ for any operator $\hat{\mathcal{O}}$ and define the storage efficiency by the ratio

$$\eta_{\text{in}} \equiv \frac{\langle \hat{\mathcal{K}}^\dagger \hat{\mathcal{K}} \rangle_{T'}}{\int_{-\infty}^{T'} \langle \hat{\mathcal{E}}_{\text{in}}^\dagger \hat{\mathcal{E}}_{\text{in}} \rangle_t dt}, \quad (37)$$

i.e., by the number of stored spin excitations divided by the number of incoming signal photons. We can use the integral relation in Eq. (E2) to express the efficiency as

$$\eta_{\text{in}} = 1 - \frac{2 \int_{-\infty}^{T'} dt \langle \frac{1}{2} \hat{\mathcal{E}}_{\text{out}}^\dagger \hat{\mathcal{E}}_{\text{out}} + \gamma_P \hat{\mathcal{P}}^\dagger \hat{\mathcal{P}} + \gamma_S \hat{S}^\dagger \hat{S} + \gamma_K \hat{\mathcal{K}}^\dagger \hat{\mathcal{K}} \rangle_t}{\int_{-\infty}^{T'} dt \langle \hat{\mathcal{E}}_{\text{in}}^\dagger \hat{\mathcal{E}}_{\text{in}} \rangle_t}. \quad (38)$$

We find that the storage efficiency is limited by four relaxation mechanisms: decoherence of excited alkali atoms at a rate γ_P , decoherence of the alkali-metal spin at a rate γ_S , decoherence of the noble-gas spin at a rate γ_K , and leakage of photons during the storage represented by $\int_{-\infty}^{T'} \langle \hat{\mathcal{E}}_{\text{out}}^\dagger \hat{\mathcal{E}}_{\text{out}} \rangle_t dt$.

B. Retrieval efficiency

The retrieval process starts at $t = T' + \tau$. During this process, there is no input field, and the spin excitations are mapped to the output field $\hat{\mathcal{K}}(T' + \tau) \rightarrow \hat{\mathcal{E}}_{\text{out}}$. The retrieval ends when no atomic excitations are left in the medium. The retrieval efficiency is then given by

$$\eta_{\text{out}} \equiv \frac{\int_{T'+\tau}^{\infty} \langle \hat{\mathcal{E}}_{\text{out}}^\dagger \hat{\mathcal{E}}_{\text{out}} \rangle_t dt}{\langle \hat{\mathcal{K}}^\dagger \hat{\mathcal{K}} \rangle_{(T'+\tau)}}, \quad (39)$$

i.e., the number of retrieved photons divided by the number of stored spin excitations. Using the integral relation in Eq. (E2), we find

$$\eta_{\text{out}} = 1 - \frac{2 \int_{T'+\tau}^{\infty} \langle \gamma_P \hat{\mathcal{P}}^\dagger \hat{\mathcal{P}} + \gamma_S \hat{S}^\dagger \hat{S} + \gamma_K \hat{\mathcal{K}}^\dagger \hat{\mathcal{K}} \rangle_t dt}{\langle \hat{\mathcal{K}}^\dagger \hat{\mathcal{K}} \rangle_\tau}. \quad (40)$$

It is evident that the retrieval efficiency is maximized if the duration for which $\hat{\mathcal{P}}$ and \hat{S} are excited is minimal.

V. OPTIMAL LIGHT STORAGE

Our motivation for setting up an interface between optical signals and noble-gas spin ensembles is to utilize the long lifetime of $\hat{\mathcal{K}}$. We aim to find controllable and reversible processes that efficiently transfer the quantum excitations from $\hat{\mathcal{E}}_{\text{in}}$ to $\hat{\mathcal{K}}$, thus maximizing η_{in} in Eq. (37). We generalize the variational technique introduced in Ref. [71] to numerically find the optimal control pulses of $\Omega(t)$, $\delta_k(t)$, and $\delta_s(t)$ that maximize the storage efficiency.

Since \hat{f}_P , \hat{f}_S , and \hat{f}_K are vacuum noise operators (see Appendix B), and since we start with a single excitation in a well-defined mode, we can simplify Eqs. (31) and (34) by setting $\hat{f}_P = \hat{f}_S = \hat{f}_K = 0$ and by replacing the quantum operators with complex numbers ($\hat{\mathcal{P}} \rightarrow \mathcal{P}$, $\hat{S} \rightarrow \mathcal{S}$, $\hat{\mathcal{K}} \rightarrow \mathcal{K}$, and $\hat{\mathcal{E}}_{\text{in}} \rightarrow \mathcal{E}_{\text{in}}$) describing the shapes of the quantum modes [61, 66].

For the numerical optimization, we choose the input signal to have an exponential temporal profile

$$\mathcal{E}_{\text{in}}(t) = A\sqrt{\frac{2}{T}}e^{(t-T)/T} \quad -2T \leq t \leq T \quad (41)$$

and zero otherwise. For Λ -type memories in the adiabatic regime, optimal storage of an exponentially-shaped signal is done with a square control pulse [61]. Therefore, this choice allows a direct comparison to simple analytic expressions for the efficiencies. The exponential signal is truncated at $t = -2T$ to reduce the numerical complexity, and $A = e^3/\sqrt{e^6 - 1}$ guarantees the normalization $\int_{-2T}^T |\mathcal{E}_{\text{in}}(t)|^2 dt = 1$.

A. Numerical protocol

The scalar version of Eqs. (31)-(34) is given by

$$\partial_t \mathcal{S} = -(\gamma_s + \Gamma_\Omega + i\delta_s)\mathcal{S} - iJ\mathcal{K} - Q\Omega^* \mathcal{E}_{\text{in}}, \quad (42)$$

$$\partial_t \mathcal{K} = -(\gamma_k + i\delta_k)\mathcal{K} - iJ\mathcal{S}. \quad (43)$$

In this analysis, $\Omega(t)$, $\delta_k(t)$, and $\delta_s(t)$ are the optimization parameters, while we set $\Delta = \gamma_k = 0$, assume that Ω is real, and take $T' - T = \pi/[2\max(\sqrt{J^2 - \gamma_s^2/4}, \gamma_s)]$. Recall that $T' - T \geq 0$ allows for interaction predominantly between the spins \mathcal{S} and \mathcal{K} after the input signal pulse ended. In the strong-coupling regime $J \gg \gamma_s$, the duration $T' - T = \pi/(2\sqrt{J^2 - \gamma_s^2/4})$ corresponds to complete transfer of the alkali spin state to the noble-gas spin.

We numerically iterate on the control functions $\Omega(t)$, $\delta_k(t)$, and $\delta_s(t)$. To determine their variations between subsequent iterations, we use the gradient ascent method following Ref. [71] and maximize the functional

$$\begin{aligned} \Phi = & \frac{1}{2}|\mathcal{K}(T')|^2 - \frac{1}{2} \int_{-\infty}^{T'} dt \left[k^* (\partial_t \mathcal{K} + (\gamma_k + i\delta_k)\mathcal{K} + iJ\mathcal{S}) \right. \\ & \left. + s^* (\partial_t \mathcal{S} + (\gamma_s + \gamma_\Omega + i\delta_s)\mathcal{S} + iJ\mathcal{K} + Q\Omega\mathcal{E}_{\text{in}}) + \text{h.c.} \right]. \end{aligned} \quad (44)$$

The functional Φ describes the number of stored excitations in the noble-gas spin $|\mathcal{K}(T')|^2$, whereas $s(t)$ and $k(t)$ are Lagrange multipliers which enforce that the equations of motion of \mathcal{S} and \mathcal{K} are satisfied. The variations in Φ with respect to the relevant functions vanish for the optimal solution. Variational calculus yields the equations of motion for the Lagrange multipliers,

$$\partial_t s = (\gamma_s + \gamma_\Omega - i\delta_s)s - iJk, \quad (45)$$

$$\partial_t k = (\gamma_k - i\delta_k)k - iJs, \quad (46)$$

with the conditions $s(T') = 0$ and $k(T') = \mathcal{K}(T')$. Note that we are interested in computing the multipliers $s(t)$ and $k(t)$ for $t \leq T'$, and therefore we numerically solve Eqs. (45)-(46) backwards in time, from $t = T'$. In every iteration, we first solve Eqs. (42)-(43), compute $\mathcal{K}(T)$,

and then solve Eqs. (45)-(46). We use these solutions to estimate the functional derivatives of the control functions $\Omega(t)$, $\delta_k(t)$, and $\delta_s(t)$

$$\frac{\partial \Phi}{\partial \tilde{\Omega}} = -2\tilde{\Omega} \text{re}(s^* \mathcal{S}) - \sqrt{\frac{2C}{C+1}} \text{re}(s) \mathcal{E}_{\text{in}}, \quad (47)$$

$$\frac{\partial \Phi}{\partial \delta_k} = \text{im}(k^* \mathcal{K}), \quad (48)$$

$$\frac{\partial \Phi}{\partial \delta_s} = \text{im}(s^* \mathcal{S}), \quad (49)$$

where we use the normalized rate $\tilde{\Omega} = \sqrt{\gamma_\Omega}$. This set of equations is used to update the control functions for the next iteration. The control functions in the n^{th} iteration are determined using the gradient ascent method with momentum [72, 73]

$$\tilde{\Omega}^{(n)} = (1 + \alpha_n)\tilde{\Omega}^{(n-1)} - \alpha_n\tilde{\Omega}^{(n-2)} + \frac{1}{\lambda_{\tilde{\Omega}}} \frac{\partial \Phi}{\partial [\tilde{\Omega}(t)]}, \quad (50)$$

$$\delta_k^{(n)} = (1 + \alpha_n)\delta_k^{(n-1)} - \alpha_n\delta_k^{(n-2)} + \frac{1}{\lambda_{\delta_k}} \frac{\partial \Phi}{\partial [\delta_k(t)]}. \quad (51)$$

$$\delta_s^{(n)} = (1 + \alpha_n)\delta_s^{(n-1)} - \alpha_n\delta_s^{(n-2)} + \frac{1}{\lambda_{\delta_s}} \frac{\partial \Phi}{\partial [\delta_s(t)]}. \quad (52)$$

Here we choose $\alpha_n = 0.9$ for $n \geq 3$ and $\alpha = 0$ otherwise.

We found the following numerical procedure to be efficient. For each optimization run, we first set $\delta_s(t) = \delta_k(t) = 0$ and optimize solely with respect to $\tilde{\Omega}(t)$. The step size $\lambda_{\tilde{\Omega}}$ is taken within the range of $[10^{-2}, 10^2]$ with longer T corresponding to smaller values of $\lambda_{\tilde{\Omega}}$. The initial guess for $\tilde{\Omega}(t)$ in the run with the maximal value of $J = J_{\text{max}}$ for each T is a constant (square) pulse for $t \leq T'$. For smaller values of $J < J_{\text{max}}$, we attempt two independent optimization procedures using different initial guesses based on the optimal solution $\tilde{\Omega}_{\text{iter},1}(t)$ previously computed for the same T and nearest J . One guess is $\tilde{\Omega}_{\text{iter},1}(t)$ up to the time in which \mathcal{K} is maximal with additional padding of zeros at the end of the pulse to account for the increase of T' due to the decrease of J . The other guess is a square pulse taking the average value of $\tilde{\Omega}_{\text{iter},1}(t)$ between $-0.5T \leq t \leq T$. For each value of J and T , we record the new initial guess $\tilde{\Omega}_{\text{iter},2}(t)$ as the solution that realizes higher storage efficiency of the two optimization attempts. We then allow the solver to vary $\delta_s(t)$ and $\delta_k(t)$ as well as $\tilde{\Omega}(t)$. We choose the steps adaptively $\lambda_{\delta_s}^{-1} = \text{mean}(\gamma_\Omega)$ and $\lambda_{\delta_k}^{-1} = \text{mean}(\gamma_J)$, according to the values of $\gamma_\Omega(t)$ and $\gamma_J(t)$ corresponding to $\tilde{\Omega}(t)$ in the previous runs [see Eqs. (66) and (67) below].

We typically observe convergence in $|\mathcal{K}(T)|^2$ after 500 iterations, except at the narrow region where both $J \gg \gamma_s$ and $\gamma_s T \gg 1$, where convergence is obtained with 5000 iterations. We also try different initial conditions, including high values of δ_k at the beginning and at the end of the pulse. We find that the shape of δ_k and δ_s has only a minor influence on the obtained efficiency, except during the memory time, where large δ_k is required for suppressing relaxation induced by the alkali spin.

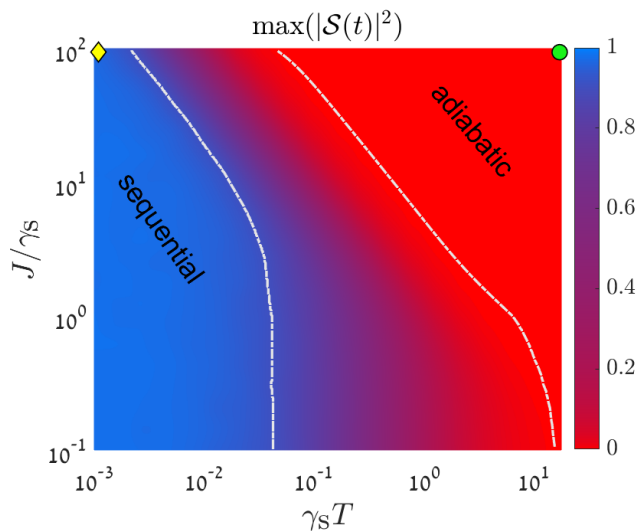


Figure 3. Maximal excitation of the alkali spin $|\mathcal{S}|^2$ during the optimal storage process. Two distinct regimes of complete excitation and no excitation are observed when varying the pulse duration $\gamma_s T$ and the degree of coupling between the alkali and noble-gas spins J/γ_s . Dashed lines denote the conditions $\max(|\mathcal{S}(t)|^2) = 0.95$ and $\max(|\mathcal{S}(t)|^2) = 0.05$ and mark the boundaries of these regimes, corresponding to the sequential and the adiabatic storage schemes. The yellow diamond denotes the optimal solution presented in Fig. 5, and the green circle denotes the optimal solution presented in Fig. 7.

B. Optimal solutions

The optimal-control solutions we find for $\Omega(t)$, $\delta_k(t)$ and $\delta_s(t)$ depend on the dimensionless parameters $\gamma_s T$, J/γ_s , and C . Interestingly, the optimal solutions differ in the degree to which the alkali coherence is excited. In Fig. 3, we plot for different values of $\gamma_s T$ and J/γ_s the maximal excitation of the alkali-spin coherence during the storage process in the optimal solutions. We find that for long optical signals $T \gg 1/J$, the alkali spins are barely excited, and the photon is directly mapped onto the noble-gas spins, whereas for shorter pulses ($T \ll 1/\gamma_s$ and $T \lesssim 1/J$) the photon is completely mapped onto the alkali spins first. The storage efficiency for both $T \gg \gamma_s/J^2$ and $J \gg \gamma_s$ approaches unity, as presented in Fig. 2(a) in Ref. [59].

We present an optimal solution for a short input pulse $T \ll 1/\gamma_s$ and $T \lesssim 1/J$ in the regime $J \gg \gamma_s$ in Fig. 5 (corresponding to the yellow diamond in Fig. 3). We find that for optimal storage, the photon is mapped rapidly onto the alkali spin and only then transferred to the noble-gas spin. We identify the regime where such sequential mapping is optimal by the condition $\max(|\mathcal{S}(t)|^2) \leq 0.95$, as presented by the dashed line in Fig. 3 and in Fig. 2(a) of Ref. [59].

We present an optimal solution in the regime $T \gg 1/J$ in Fig. 7 (corresponding to the green circle in Fig. 3).

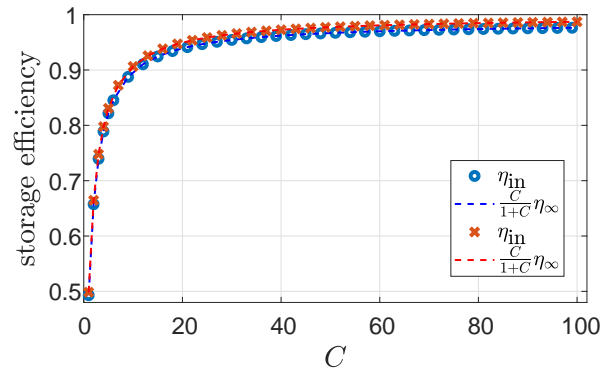


Figure 4. Expected scaling $\eta_{\text{in}} = \eta_{\infty} C / (C + 1)$ (dashed lines) of the storage efficiency η_{in} with the cooperativity C , verified numerically using $J = 100\gamma_s$ and $\gamma_s T = 10^{-3}$ for the sequential storage scheme (circles) and $\gamma_s T = 17.8$ for the adiabatic storage scheme (crosses).

Here the alkali spin is barely excited, and, via adiabatic variation of the control field, the signal is directly mapped onto the noble-gas spin. We identify the regime where such adiabatic mapping is optimal by the condition $\max(|\mathcal{S}(t)|^2) \leq 0.05$, as presented by the dashed line in Fig. 3 and in Fig. 2(a) of Ref. [59]. We analytically analyze the sequential and adiabatic mapping schemes in Secs. VI and VII, respectively.

Furthermore, we find numerically that the efficiency is maximal at $\delta_s(t) = 0$ for the sequential mapping and is independent of δ_s for the adiabatic mapping. We elaborate on this in Appendix G.

Finally we note that the value of C was not varied in the above analysis, as its effect can be accounted for by simply scaling the storage efficiency according to $\eta_{\text{in}} = \eta_{\infty} C / (C + 1)$, where η_{∞} is the storage efficiency for $C \rightarrow \infty$, as presented in Ref. [59]. We verify this scaling law in Fig. 4 for the adiabatic and sequential solutions.

VI. SEQUENTIAL MAPPING

We first analyze the sequential mapping, which is found optimal for storage of short pulses satisfying $T \ll 1/\gamma_s$ and $T \lesssim 1/J$. In this mapping scheme, as exemplified in Fig. 5, storage is conducted by a sequential two-stage transfer of the excitation $\hat{\mathcal{E}}_{\text{in}} \rightarrow \hat{\mathcal{S}}(T) \rightarrow \hat{\mathcal{K}}(T')$, by first mapping the signal onto the alkali spin $\hat{\mathcal{S}}$ at time T , and afterwards mapping it onto the noble-gas spin $\hat{\mathcal{K}}$ at time T' . Below we describe these two stages in detail.

We simplify the discussion of the sequential mapping by neglecting the slow relaxation of the noble-gas spins (*i.e.*, setting $\gamma_k = 0$) during the mapping processes. We retain γ_k only for the long memory time.

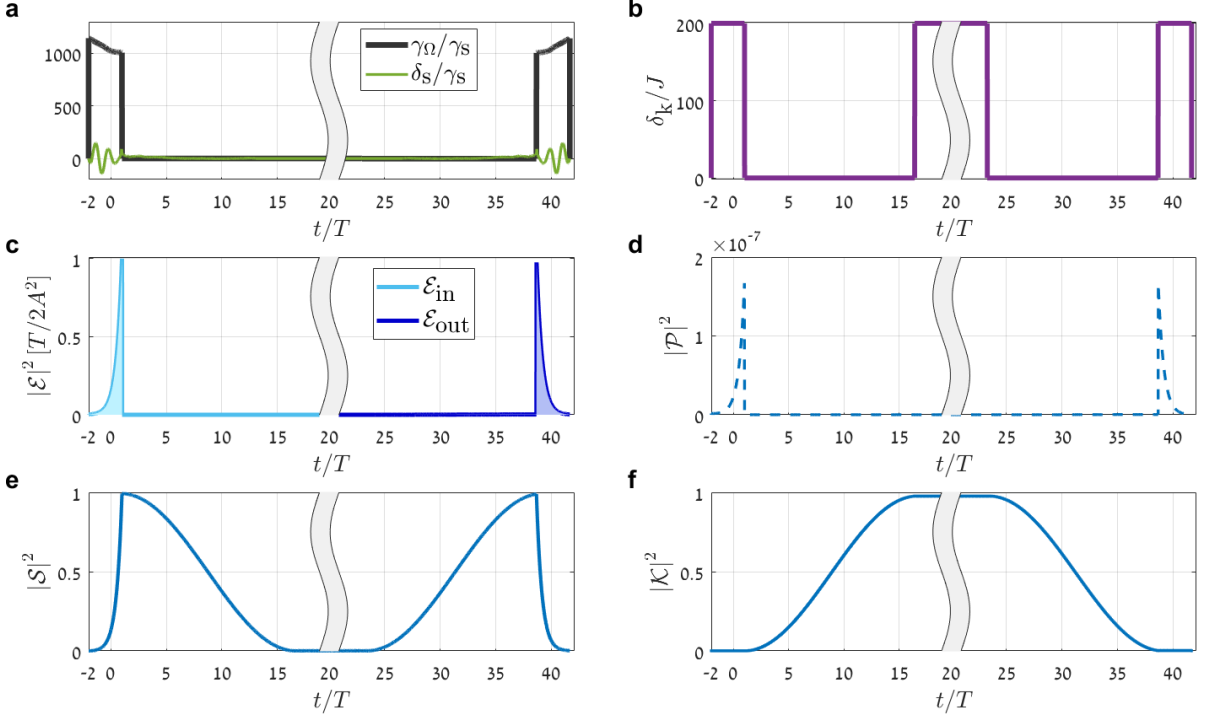


Figure 5. Numerically-optimized quantum memory operation in the sequential mapping regime. Here $J = 100\gamma_s$ and $\gamma_s T = 10^{-3}$, and we find a memory efficiency of $\eta_{\text{tot}} = 0.95$ for $C = 100$. We show the obtained γ_Ω , δ_s , δ_k , $|\mathcal{E}_{\text{in}}|^2$, $|\mathcal{E}_{\text{out}}|^2$, $|\mathcal{P}|^2$, $|\mathcal{S}|^2$, and $|\mathcal{K}|^2$ of the optimal solution. In the first stage $-2T \leq t \leq T$, the control field drives the system, and the input pulse is mapped onto the collective state of the alkali spins, while the noble gas is detuned away by a large δ_k . In the second stage $T < t \leq T'$ (here $T'/T = 15$), by tuning $\delta_s = \delta_k = 0$, the alkali spins exchange the excitation with the noble-gas spins. Subsequently, the noble-gas spins are decoupled from the alkali spins by increasing δ_k . The optical signal is retrieved by time reversing the storage sequence, except for a correction of order $\gamma_s T$ to the control field amplitude $\gamma_\Omega(\text{retrieval}) = \gamma_\Omega(\text{storage}) - 2\gamma_s$, which corrects for the effect of nonzero alkali-spin relaxation to first order, as described in the text.

A. Storage stage 1: $\hat{\mathcal{E}}_{\text{in}} \rightarrow \hat{\mathcal{S}}$

In the first stage, the solution in Fig. 5 suggests that $\Omega(t)$ stimulates the coherent absorption of the signal, while δ_k is kept large. For $\delta_k \gg J, T^{-1}$ we indeed find from Eq. (34) that $\hat{\mathcal{K}} \approx (J/\delta_k)\hat{\mathcal{S}}$, such that $\langle \hat{\mathcal{K}}^\dagger \hat{\mathcal{K}} \rangle \ll 1$. Therefore, large δ_k efficiently decouples the noble-gas spins, rendering the first storage stage similar to standard light storage onto alkali spins.

In Appendix F, we review the process of light storage onto and retrieval from alkali spins, following Ref. [61]. The maximal efficiency of the process $\hat{\mathcal{E}}_{\text{in}} \rightarrow \hat{\mathcal{S}}$ is given in Eq. (F7) for a general pulse shape and optimally shaped control. For the particular case of exponentially-shaped signal, a square control pulse with a constant value of $\gamma_\Omega = 1/T + \gamma_s$ maximizes the storage efficiency, which reads

$$\eta_{\text{in}}^{(\mathcal{E} \rightarrow \mathcal{S})} = \frac{\langle \hat{\mathcal{S}}^\dagger \hat{\mathcal{S}} \rangle_T}{\int_{-\infty}^T \langle \hat{\mathcal{E}}_{\text{in}}^\dagger \hat{\mathcal{E}}_{\text{in}} \rangle_t dt} = \frac{C}{C+1} \cdot \frac{1}{1 + \gamma_s T}. \quad (53)$$

This matches the optimal efficiency we find numerically for this storage process in the sequential regime. Note

that, for a general pulse shape of characteristic duration T and characteristic bandwidth $1/T$, Eq. (53) provides a rough estimate for the storage efficiency.

B. Storage stage 2: $\hat{\mathcal{S}} \rightarrow \hat{\mathcal{K}}$

In the second stage, as shown in Fig. 5, the control field is turned off ($\Omega = 0$), and the excitation is coherently transferred from the alkali to the noble-gas spins $\hat{\mathcal{S}}(T) \rightarrow \hat{\mathcal{K}}(T')$ via the spin-exchange interaction. In general, the dynamics of spin-exchange in the presence of diffusion is multi-mode [57, 63], and we present the complete multi-mode calculation in Appendix H. Here we present the approximated dynamics for the uniform modes. This solution is accurate for anti-relaxation coated cells [63].

The exchange evolution of the alkali and noble-gas spins over the duration $T_\pi = T' - T$ is given by

$$\begin{aligned} \hat{\mathcal{S}}(T') = & e^{-\frac{1}{2}(i\delta_s + i\delta_k + \gamma_s)T_\pi} \left\{ -\frac{iJ}{\tilde{J}} \sin(\tilde{J}T_\pi) \hat{\mathcal{K}}(T) \right. \\ & \left. + \left[\cos(\tilde{J}T_\pi) - \frac{\gamma_s - i\delta}{2\tilde{J}} \sin(\tilde{J}T_\pi) \right] \hat{\mathcal{S}}(T) \right\} + \hat{\mathcal{W}}_s(T_\pi) \end{aligned} \quad (54)$$

for the alkali spins and

$$\hat{\mathcal{K}}(T') = e^{-\frac{1}{2}(i\delta_s + i\delta_k + \gamma_s)T_\pi} \left\{ -\frac{iJ}{\tilde{J}} \sin(\tilde{J}T_\pi) \hat{\mathcal{S}}(T) \right. \\ \left. + \left[\cos(\tilde{J}T_\pi) + \frac{\gamma_s - i\delta}{2\tilde{J}} \sin(\tilde{J}T_\pi) \right] \hat{\mathcal{K}}(T) \right\} + \hat{\mathcal{W}}_k(T_\pi) \quad (55)$$

for the noble-gas spins. Here

$$\delta = \delta_k - \delta_s \quad (56)$$

is the mismatch between the spin precession frequencies, and

$$\tilde{J} = \sqrt{J^2 + (\delta + i\gamma_s)^2/4} \quad (57)$$

denotes the effective exchange rate. The stochastic quantum processes $\hat{\mathcal{W}}_s$ and $\hat{\mathcal{W}}_k$ for the alkali and noble-gas spins are defined in Appendix H.

Maximal exchange rate and thus optimal transfer $\hat{\mathcal{S}}(T) \rightarrow \hat{\mathcal{K}}(T')$ are obtained by setting $\delta(B) = 0$ for the entire exchange time T_π . To simplify the analysis at this point, we consider the particular regime of strong coupling $J \gg \gamma_s$, where efficient exchange between the spin gases, and therefore high storage efficiency, can be realized. In this regime, we set $T_\pi \approx (\frac{\pi}{2}\tilde{J} - \gamma_s)/\tilde{J}^2$ and get, to leading order in γ_s/J ,

$$\hat{\mathcal{K}}(T') = e^{-\frac{\pi\gamma_s}{4J}} \hat{\mathcal{S}}(T) + \hat{\mathcal{W}}_k(T_\pi), \quad (58)$$

which we substitute into Eq. (39) to obtain the optimal storage efficiency for the second stage

$$\eta_{\text{in}}^{(S \rightarrow \mathcal{K})} = \exp\left(-\frac{\pi\gamma_s}{2J}\right). \quad (59)$$

C. Memory time

Once the excitation is stored on the uniform mode of the noble-gas spins, we can decouple the state of the two spin ensembles by applying a large magnetic field. Specifically, we take $\delta(B) \gg J$, such that $\tilde{J} \approx \delta/2$, and Eq. (55) becomes

$$\hat{\mathcal{K}}(T' + \tau) = e^{-(i\delta_k + \gamma_k)\tau} \hat{\mathcal{K}}(T') + \hat{\mathcal{W}}' \quad (60)$$

for the memory time τ , where $\hat{\mathcal{W}}' = \hat{\mathcal{W}}_k(T' + \tau) - \hat{\mathcal{W}}_k(T')$. The noble-gas spins then act as a quantum memory that decays according $\eta_{\text{dark}}(\tau)$ in Eq. (36), with potentially very long lifetime γ_k^{-1} .

D. Retrieval: $\hat{\mathcal{K}} \rightarrow \hat{\mathcal{S}} \rightarrow \hat{\mathcal{E}}_{\text{out}}$

We retrieve the photons from the memory by realizing the process $\hat{\mathcal{K}}(T' + \tau) \rightarrow \hat{\mathcal{S}}(T' + \tau + T_\pi) \rightarrow \hat{\mathcal{E}}_{\text{out}}$. First, the magnetic field is tuned to strongly couple the two spin

gases by setting $\delta(B) = 0$. As described by Eq. (54), the excitation is mapped back from the noble gas to the alkali spins after the same transfer time T_π

$$\langle \hat{\mathcal{S}}^\dagger \hat{\mathcal{S}} \rangle_{t_r} = e^{-\frac{\pi\gamma_s}{2\tilde{J}}} \langle \hat{\mathcal{K}}^\dagger \hat{\mathcal{K}} \rangle_{(T'+\tau)}, \quad (61)$$

where $t_r = T' + \tau + T_\pi$, yielding the retrieval efficiency of $\eta_{\text{out}}^{(\mathcal{K} \rightarrow \mathcal{S})} = \eta_{\text{in}}^{(S \rightarrow \mathcal{K})}$. Retrieval of the photons from the alkali spins is then performed as a standard retrieval in Λ -system memories, as reviewed in Appendix F. Importantly, the temporal mode of the output field is determined by the temporal shape of the control. Therefore, emission into a desired temporal mode can be realized by shaping the control field [61].

Here we consider retrieval into a temporal mode that is the time-reverse of the input signal $\mathcal{E}_{\text{out}}(t) \propto \mathcal{E}_{\text{in}}^*(t_r + T - t)$. For $\gamma_s = 0$, the retrieval is realized with efficiency $C/(C + 1)$ by the exact time-reversal of the storage sequence. For nonzero γ_s , one can still shape the retrieval control field to achieve retrieval into the desired output mode [provided that this mode does not have an infinite tail with amplitude decaying slower than $\exp(-\gamma_s t)$] [61], but the retrieval efficiency becomes mode-dependent, as given in Eq. (F10). Nevertheless, in the regime $\gamma_s \ll 1/T$, to first order in $\gamma_s T$, the efficiency of retrieval into $\mathcal{E}_{\text{in}}^*(t_r + T - t)$ is equal to the efficiency of storing $\mathcal{E}_{\text{in}}(t)$ [cf. Eqs. (F7) and (F10)].

For exponentially-shaped signals satisfying $T < 1/\gamma_s$, retrieval into $\mathcal{E}_{\text{in}}^*(t_r + T - t)$ is realized using a constant control field with $\gamma_\Omega = 1/T - \gamma_s$ [compare to $\gamma_\Omega = 1/T + \gamma_s$ during optimal storage of exponentially shaped $\mathcal{E}_{\text{in}}(t)$] and yields the retrieval efficiency

$$\eta_{\text{out}}^{(S \rightarrow \mathcal{E})} = \frac{\int_{t_r}^{\infty} \langle \hat{\mathcal{E}}_{\text{out}}^\dagger \hat{\mathcal{E}}_{\text{out}} \rangle_t dt}{\langle \hat{\mathcal{S}}^\dagger \hat{\mathcal{S}} \rangle_{t_r}} = \frac{C}{C + 1} (1 - \gamma_s T) \quad (62)$$

[compare to Eq. (53) for storage].

VII. ADIABATIC MAPPING

We now turn to analyze the adiabatic mapping, which is found optimal at the long-pulse regime $T \gg 1/J$. In this mapping scheme, as exemplified in Fig. 7, $\hat{\mathcal{S}}$ is kept unexcited during the storage and retrieval to avoid the loss of excitations by the alkali-spin relaxation [cf. Eq. (40)]. The principle is that $\hat{\mathcal{S}}$ can mimic the dynamics of $\hat{\mathcal{P}}$ in the adiabatic regime, thus serving as a mediator whose excitation is negligible.

During the storage time $t \leq T' = T$, we set $\delta_s(B) = \delta_k(B) = 0$ and apply an optimal pulse-shape of $\Omega(t)$, as shown in Fig. 7. This establishes a direct coherent mapping between the optical field and the noble-gas spins $\hat{\mathcal{E}}_{\text{in}} \rightarrow \hat{\mathcal{K}}(T)$. Similarly, retrieval employs the direct mapping $\hat{\mathcal{K}}(T + \tau) \rightarrow \hat{\mathcal{E}}_{\text{out}}$.

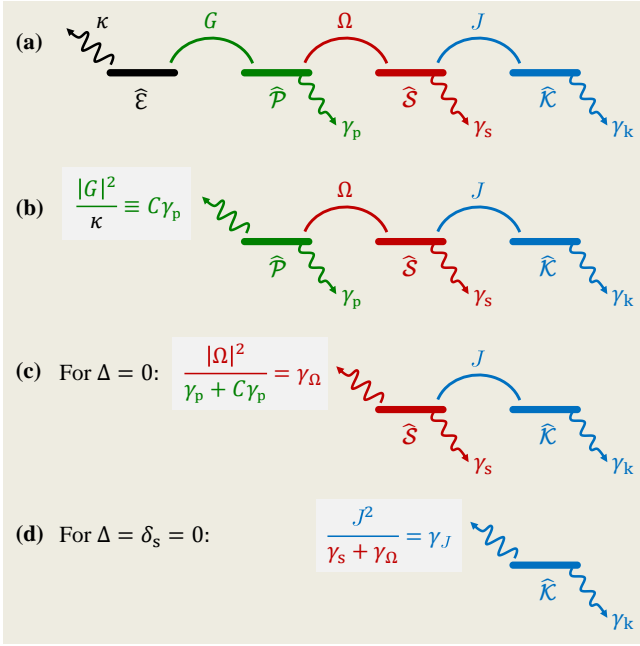


Figure 6. Emergence of a decay rate γ_J from the collective noble-gas spin \hat{K} during adiabatic retrieval. The picture is similar for adiabatic storage. (a) The optical cavity field $\hat{\mathcal{E}}$ couples to the collective optical dipole $\hat{\mathcal{P}}$, which couples to the collective alkali spin $\hat{\mathcal{S}}$, which couples to the collective noble-gas spin \hat{K} , with corresponding rates G , Ω , and J . The optical field decays into the desired output field $\hat{\mathcal{E}}_{\text{out}}$ with rate κ . The rates γ_p , γ_s , and γ_k encompass both relaxation and coupling to other (undesired) modes (not shown). (b) In the fast-cavity limit ($\kappa \gg G$), the cavity field adiabatically follows the optical dipole, giving rise to a decay rate $C\gamma_p$ from the optical dipole into the output field. This “good” decay rate $C\gamma_p$ competes with “bad” decay rate γ_p , contributing a factor of $C\gamma_p/(C\gamma_p + \gamma_p)$ to the retrieval efficiency. (c) For moderate control fields ($C\gamma_p \gg \Omega$), the optical dipole adiabatically follows the alkali spin, giving rise to a decay rate γ_Ω from the alkali spin. This “good” decay rate γ_Ω competes with “bad” decay rate γ_s , contributing a factor of $\gamma_\Omega/(\gamma_\Omega + \gamma_s)$ to the retrieval efficiency. (d) For $\gamma_\Omega + \gamma_s \gg J$ (corresponding to $T \gg 1/J$, since $T \sim 1/\gamma_J$), the alkali spin adiabatically follows the noble-gas spin, giving rise to a decay rate γ_J from the noble gas spin. This “good” decay rate γ_J competes with “bad” decay rate γ_k , contributing a factor of $\gamma_J/(\gamma_J + \gamma_k)$ to the retrieval efficiency.

A. Adiabatic equations of motion

We consider the dynamics of the uniform mode $\hat{\mathcal{S}}(t)$ in the adiabatic regime $\gamma_\Omega \gg J$, $|Q\Omega|$. Eq. (31) can then be approximated by

$$\hat{\mathcal{S}} = -\frac{Q\Omega^*\hat{\mathcal{E}}_{\text{in}} + iJ\hat{K} - \hat{F}_S}{\Gamma_\Omega + \gamma_s + i\delta_s}. \quad (63)$$

Here $\hat{\mathcal{S}}(t)$ adiabatically follows the operators \hat{K} , $\hat{\mathcal{E}}_{\text{in}}$, and \hat{F}_S , similarly to the role of $\hat{\mathcal{P}}$ in Eq. (C2). The alkali-spin excitation is small $\langle \hat{\mathcal{S}}^\dagger \hat{\mathcal{S}} \rangle \leq J^2/|\Gamma_\Omega|^2 \ll 1$, allowing for

high memory efficiency according to Eqs. (38) and (40). By substituting the adiabatic solution (63) in Eqs. (29)-(30) and in Eq. (34), we obtain

$$\hat{\mathcal{E}}_{\text{out}} = (\alpha - ia_J Q\Omega/J)\hat{\mathcal{E}}_{\text{in}} + a_J(\Omega/\Omega^*)\hat{K} + \hat{F}_\mathcal{E}, \quad (64)$$

$$\partial_t \hat{K} = -(\gamma_k + \Gamma_J + i\delta_k)\hat{K} + a_J\hat{\mathcal{E}}_{\text{in}} + \hat{F}_K. \quad (65)$$

Here we define the stimulated coupling rate to the noble-gas spins as

$$\Gamma_J(t) \equiv \frac{J^2}{\Gamma_\Omega(t) + \gamma_s + i\delta_s(t)}, \quad (66)$$

as well as the parameter $a_J \equiv iQ\Omega^*\Gamma_J/J$. The vacuum noise operators are $\hat{F}_K = \hat{f}_K - i\Gamma_J\hat{F}_S/J$ and $\hat{F}_\mathcal{E} = \hat{f}_\mathcal{E} + ia_J\Omega\hat{F}_S/(J\Omega^*)$, and the parameters Q and α are defined in Eqs. (33) and (C5). The imaginary part $\text{im}(\Gamma_J)$ constitutes the frequency shift due to the spin-exchange coupling to the alkali spins, which vanishes when operating at $\Delta = \delta_s = 0$. The real part

$$\gamma_J \equiv \text{re}(\Gamma_J) \quad (67)$$

constitutes the relaxation inherited from the alkali spins. The alkali spins themselves experience a relaxation at a high rate $\gamma_\Omega + \gamma_s$, composed of radiative (γ_Ω) and non-radiative (γ_s) losses; both are partially inherited by the noble gas and are accounted for in γ_J . The emergence of γ_J and its analogy to γ_Ω are illustrated in Fig. 6 for the case of retrieval. The intuition is the same for the case of storage.

Equation (65) is a linear stochastic differential equation and, similarly to Eq. (F1), can be solved by

$$\hat{K}(t) = \Upsilon_{t,-\infty}\hat{K}(-\infty) + \int_{-\infty}^t h_J(t,s)\hat{\mathcal{E}}_{\text{in}}(s)ds + \hat{W}_K(t), \quad (68)$$

where $h_J(t,s) = \Upsilon_{t,s}a_J(s)$, and $\hat{W}_K(t) = \int_{-\infty}^t \Upsilon_{t,s}\hat{F}_K(s)ds$, and the evolution function from time t' to time t is

$$\Upsilon_{t,t'} = e^{-\int_{t'}^t [\gamma_k + \Gamma_J(s) + i\delta_k(s)]ds}. \quad (69)$$

Below we estimate the efficiencies of the storage and retrieval stages.

B. Storage: $\hat{\mathcal{E}}_{\text{in}} \rightarrow \hat{K}$

The spins are initially unexcited $\langle \hat{K}^\dagger \hat{K} \rangle_{-\infty} = 0$, so the first term in Eq. (68) vanishes. We therefore get

$$\hat{K}(T) = \int_{-\infty}^T h_J(T,s)\hat{\mathcal{E}}_{\text{in}}(s)ds + \hat{W}_K(T). \quad (70)$$

The transfer function h_J satisfies the inequality

$$\int_{-\infty}^T \frac{1}{\dot{\eta}(t)} |h_J(T,t)|^2 dt \leq 1, \quad (71)$$

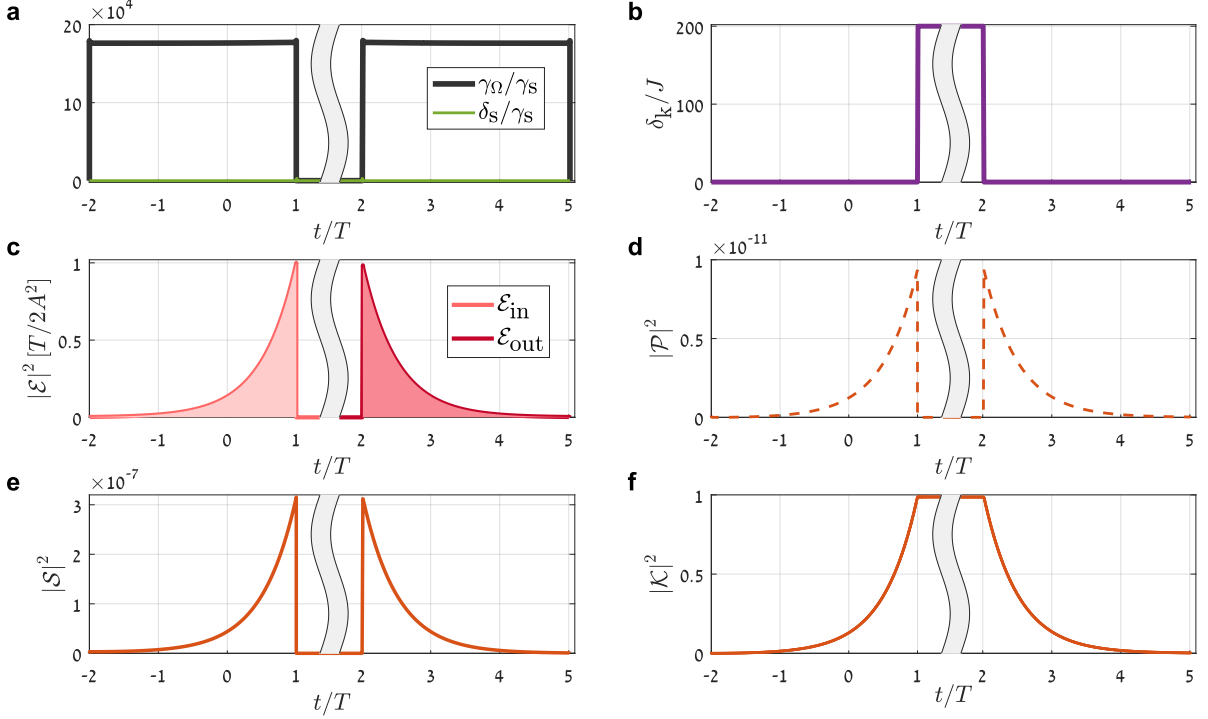


Figure 7. Numerically-optimized quantum memory operation in the adiabatic mapping regime. Here $J = 100\gamma_s$ and $\gamma_s T = 17.8$, and we find a total memory efficiency of $\eta_{\text{tot}} = 0.975$ for $C = 100$. We show the obtained γ_Ω , δ_s , δ_k , $|\mathcal{E}_{\text{in}}|^2$, $|\mathcal{E}_{\text{out}}|^2$, $|\mathcal{P}|^2$, $|\mathcal{S}|^2$, and $|\mathcal{K}|^2$ of the optimal solution. Here the noble-gas spins adiabatically follow the input optical pulse, maintaining $|\mathcal{S}|^2 \ll 1$. The optical pulse is retrieved by time reversing the storage sequence.

where the weight factor $\hat{\eta}$ is given by

$$\hat{\eta}(t) = \frac{C}{C+1} \frac{\gamma_\Omega(t)}{\gamma_\Omega(t) + \gamma_s} \frac{\gamma_J(t)}{\gamma_J(t) + \gamma_k}. \quad (72)$$

As in standard Λ -system storage (Appendix F), optimal storage is realized by shaping the control pulse to satisfy $h_J(T, t) = A_J \mathcal{E}_{\text{in}}^*(t)$ and setting $\Delta = \delta_s = \delta_k = 0$ (cf. Appendix G). The normalization constant A_J is given by

$$A_J = \sqrt{\frac{\int_{-\infty}^T |h_J(T, s)|^2 ds}{\int_{-\infty}^T \langle \mathcal{E}_{\text{in}}^\dagger \mathcal{E}_{\text{in}} \rangle_s ds}}. \quad (73)$$

Importantly, even for $\gamma_k = 0$, the storage efficiency of the adiabatic scheme depends on the particular temporal shape of the pulse being stored for any nonzero γ_s . This result stems from the time dependency of $\hat{\eta}(t)$.

We now calculate the storage efficiency for the particular mode function of an exponentially-shaped signal for negligible spin relaxation of the noble gas, $\gamma_k = 0$. As expected, we find numerically (see Fig. 7) that a constant control pulse (*i.e.*, constant γ_Ω) is optimal for $T > \gamma_s/J^2$. Substituting in Eqs. (37) and (70) the constant values $\gamma_\Omega = J^2 T - \gamma_s$ and $\gamma_J = 1/T$ yields the storage efficiency

$$\eta_{\text{in}} = \frac{C}{C+1} \left(1 - \frac{\gamma_s}{J^2 T}\right). \quad (74)$$

Turning off the control beam and applying a large magnetic field [$\delta(B) \gg J$] after storage decouples the two spin gases and lets the noble gas act as a quantum memory, free of alkali-induced relaxation.

C. Retrieval: $\hat{K} \rightarrow \hat{\mathcal{E}}_{\text{out}}$

During retrieval, starting from $t = T + \tau$, there is no input signal ($\langle \hat{\mathcal{E}}_{\text{in}}^\dagger \hat{\mathcal{E}}_{\text{in}} \rangle = 0$), and so the second term in Eq. (68) vanishes. The noble-gas spin excitations are then given by

$$\langle \hat{\mathcal{K}}^\dagger \hat{\mathcal{K}} \rangle_t = e^{-2 \int_{T+\tau}^t [\gamma_k + \gamma_J(s)] ds} \langle \hat{\mathcal{K}}^\dagger \hat{\mathcal{K}} \rangle_{(T+\tau)}, \quad (75)$$

and substitution in Eq. (64) yields the total output photon number

$$\int_{T+\tau}^{\infty} \langle \hat{\mathcal{E}}_{\text{out}}^\dagger \hat{\mathcal{E}}_{\text{out}} \rangle_{\nu} dt' = \int_{T+\tau}^{\infty} |a_J(t')|^2 \langle \hat{\mathcal{K}}^\dagger \hat{\mathcal{K}} \rangle_{\nu} dt'. \quad (76)$$

Similarly to Λ -system storage, the temporal shape of the output mode depends on the control field via the term $a_J(t')$. Substituting Eq. (76) in Eq. (39) yields the output efficiency

$$\eta_{\text{out}} = \frac{C}{C+1} \int_0^{y(\infty)} \frac{\gamma_\Omega(y)}{\gamma_\Omega(y) + \gamma_s} \frac{\gamma_J(y)}{\gamma_J(y) + \gamma_k} e^{-y} dy, \quad (77)$$

where

$$y(t) = 2 \int_{T+\tau}^t (\gamma_J(s) + \gamma_k) ds. \quad (78)$$

Therefore for nonzero γ_s and γ_k , the retrieval efficiency again depends on the specific temporal mode function of the retrieved pulse.

For the particular example of an exponentially-shaped pulse $\mathcal{E}_{\text{in}}(t)$ and $\gamma_k = 0$, as presented in Fig. 7, we use the time-reversed storage sequence with the constant values $\gamma_J = 1/T$ and $\gamma_\Omega = J^2T - \gamma_s$ to retrieve into the output mode $\mathcal{E}_{\text{out}}(t) \propto \mathcal{E}_{\text{in}}^*(\tau + T - t)$. Plugging these values into Eq. (77) and assuming $y(\infty) \gg 1$, we find

$$\eta_{\text{out}} = \eta_{\text{in}} = \frac{C}{C+1} \left(1 - \frac{\gamma_s}{J^2T}\right). \quad (79)$$

VIII. COMPARISON BETWEEN THE SEQUENTIAL AND ADIABATIC MAPPINGS

In this section, we compare the two mapping schemes by summarizing the results of Secs. VI and VII for the exponentially-shaped signal in the limit $\gamma_k T \lll 1$ (*i.e.*, we account for nonzero γ_k only during the long memory time between storage and retrieval). For the sequential mapping scheme, the memory efficiency is determined by combining Eqs. (35), (36), (53), (59), and (62) into $\eta_{\text{tot}} = \eta_{\text{in}}^{(\mathcal{E} \rightarrow \mathcal{S})} \eta_{\text{in}}^{(\mathcal{S} \rightarrow \mathcal{K})} \eta_{\text{dark}}^{(\mathcal{K} \rightarrow \mathcal{S})} \eta_{\text{out}}^{(\mathcal{S} \rightarrow \mathcal{E})}$, yielding

$$\eta_{\text{tot}} = \left(\frac{C}{C+1}\right)^2 \left(\frac{1 - \gamma_s T}{1 + \gamma_s T}\right) e^{-\frac{\pi \gamma_s}{J}} e^{-2\gamma_k \tau}. \quad (80)$$

For the adiabatic mapping scheme, the memory efficiency is determined by combining Eqs. (74) and (79),

$$\eta_{\text{tot}} = \left(\frac{C}{C+1}\right)^2 \left(1 - \frac{\gamma_s}{J^2T}\right)^2 e^{-2\gamma_k \tau}. \quad (81)$$

The memory efficiencies of both schemes approach unity for large cooperativity ($C \gg 1$) and slow alkali relaxation. The latter amounts to the condition $\gamma_s \ll J, 1/T$ in the sequential scheme, and to $\gamma_s \ll J^2T$ in the adiabatic scheme.

Equations (80) and (81) also stand as approximations for the memory efficiency of a general signal with finite duration $\sim T$ and finite bandwidth $\sim 1/T$. Notably, when the pulse is long ($T \gg J^2/\gamma_s$), the efficiency for the adiabatic scheme approaches $C^2/(C+1)^2$, whereas, for the sequential mapping, it is further reduced by the factor $\exp(-\pi\gamma_s/J)$. On the other hand when the pulse is short ($\gamma_s T \ll 1$), the memory efficiency of the sequential scheme becomes independent of the pulse duration (as long as $TC\gamma_p \gg 1$), while the efficiency of the adiabatic scheme decreases as $[1 - \gamma_s/(J^2T)]^2$ for $JT \gg 1$.

Consequently, for short pulses which satisfy the adiabatic condition $1/\gamma_s \gg T \gg 1/J$ (realizable in the

strong-coupling regime $J \gg \gamma_s$), the optimal solution is the adiabatic mapping. Interestingly, the adiabatic scheme can reach high efficiencies even when the alkali and noble-gas spins are weakly coupled and the alkali relaxation is significant $\gamma_s \gtrsim J$.

IX. POSSIBLE EXPERIMENTAL CONFIGURATIONS

The proposed quantum memory can be realized under a variety of experimental conditions. We consider two types of configurations, which differ in the pressure range of the buffer gas; here ‘buffer gas’ includes both the noble gas used as the memory and possibly additional inert gases. The first type of configurations is characterized by a high buffer-gas pressure, such that the hyperfine structure of the alkali atoms is optically unresolved and appears as a single line. The second type is characterized by a low buffer-gas pressure, such that the alkali transitions are optically resolved and allow for optical access to the different hyperfine levels. High-pressure configurations benefit from higher SEOP efficiency and thus better noble-gas hyperpolarization, from increased collective exchange rate J , and lower destruction rate γ_{diff} [cf. Eq. (C15)]. However, when the hyperfine structure is unresolved, storage via standard Λ -system processes (corresponding, *e.g.*, to EIT or to Raman absorption), are susceptible to increased four-wave mixing which compromises the memory efficiency and fidelity [35]. These configurations are therefore limited to storage via the Faraday interaction in a double-pass configuration [74, 75], which provides for a beam-splitter-like Hamiltonian without four-wave mixing. We also note that, at high buffer-gas pressure, the affect of tensor polarizability becomes negligible [60, 76], rendering the Faraday interaction with the orientation moment dominant. Low-pressure configurations benefit from strong atom-photon interaction and enable employment of standard storage processes. As diffusion is faster in these configurations, anti-relaxation coated cells should be used to avoid alkali-spin relaxation by collisions with the cell walls [8, 18, 35]. Here we analyze some exemplary possible configurations which are also summarized in Table I.

A. High buffer-gas pressure

Mixture of potassium and helium-3.— The first configuration we consider consists of a K-³He mixture enclosed in a spherical glass cell with a 1 cm radius. We consider a ³He density of $n_b = 2 \times 10^{20} \text{ cm}^{-3}$ (corresponding to 7.5 atm at ambient conditions), an alkali-metal density of $n_a = 3.5 \times 10^{14} \text{ cm}^{-3}$ (corresponding to the vapor pressure at a temperature of 220°C) and 30 Torr of N₂ to mitigate radiation trapping. The alkali spins are initial-

#	Pressure	Noble gas	Alkali	Temperature [°C]	Additional buffer gas	Coating	γ_s [1/s]	J [1/s]	C	$1/\gamma_k$	Efficiency
(1)	High	^3He , 7.5 atm	K	220	N_2 , 30 Torr	-	17	1000	100	100 [h]	97% adiabatic 93% sequential
(2)	High	^{129}Xe , 7 Torr	Rb	150	N_2 , 1500 Torr	-	6800	580	100	22 [s]	86% adiabatic
(3)	Low	^{129}Xe , 0.2 Torr	Cs	70	-	Paraffin	85	15	60	540 [s]	85% adiabatic
(4)	Low	^{129}Xe , 0.2 Torr	Cs	90	-	Alkane	50	29	100	140 [s]	94% adiabatic

Table I. **Possible experimental configurations and memory efficiencies. (1-2) High pressure configurations.** (1) Mixture of potassium, helium-3, and N_2 (the last for mitigating radiation trapping during optical pumping) in a spherical glass cell with a 1 cm radius. The noble-gas spin state potentially lives for $1/\gamma_k = 100$ hours, limited by the dipole-dipole limit. This configuration is compatible with both the sequential and adiabatic storage schemes. (2) Mixture of rubidium, xenon-129, and N_2 (the last to increase the molecular breakdown rate) in a cubical glass cell with a 1 cm edge-length. Here $J < \gamma_s$ such that the scheme is only suitable for an adiabatic operation. Here γ_k is limited by collisions with the alkali atoms. For the high-pressure configurations (1-2), mapping of the optical signal on the alkali spins can be implemented via Faraday teleportation in a double-pass configuration, which realizes a beamsplitter interaction. **(3-4) For the low-pressure configurations,** we consider a Cs- ^{129}Xe mixture enclosed in a cylindrical cell with anti-relaxation coating for the alkali spins, where γ_k is limited by collisions with the alkali atoms. For these configurations mapping of the optical signal onto the orientation moment of the alkali spins can be implemented using any standard mapping scheme, such as EIT of linearly polarized light tuned to the $F = 4 \rightarrow F = 3$ optical transition of the D1 line [35]. (3) Paraffin coating, which allows for $N_e = 1000$ bounces before spin randomization. (4) Alkane coating, which allows for $N_e = 10^5$ wall bounces before spin randomization..

ized with high spin polarization $p_a \geq 95\%$ using standard optical-pumping [17, 60], and the noble-gas spins are hyperpolarized to $p_b \gtrsim 75\%$ by SEOP [40]. The noble-gas spin state potentially lives for $1/\gamma_k = 100$ hours, limited by self dipole-dipole interactions, as long as magnetic-field inhomogeneities are minimized [40, 77]. These parameters yield $J = 1000 \text{ s}^{-1}$, $\gamma_s = 17 \text{ s}^{-1}$ (dominated by collisions with the background gas and the cell walls) [57, 60] and an expected on-resonant optical depth of $\text{OD} \approx 100$. For a cavity with a finesse $\mathcal{F} \sim 6$, we should then expect $C \approx \text{OD}\mathcal{F}/(2\pi) \approx 100$ [66]. The Faraday interaction in a double-pass configuration should be employed to map the photons onto the orientation moment of the alkali spin \hat{S} via direct interaction with the electron spin [17]. This configuration is compatible with both the sequential and adiabatic storage schemes. We calculate a total efficiency of $\eta_{\text{tot}} = 93\%$ for the sequential scheme with a high-bandwidth single-photon signal ($\gamma_\Omega = 10^4 \text{ s}^{-1}$), and $\eta_{\text{tot}} = 97\%$ for the adiabatic scheme with longer pulses.

Mixture of rubidium and xenon-129. — The second configuration contains a Rb- ^{129}Xe mixture enclosed in a cubical glass cell with a 1 cm edge-length. We consider a ^{129}Xe density of $n_b = 2.5 \times 10^{17} \text{ cm}^{-3}$ (7 Torr), an alkali density of $n_a = 10^{14} \text{ cm}^{-3}$ (temperature 150°C), and 1500 Torr of N_2 to mitigate radiation trapping and increase the molecular breakdown rate of short-lived XeRb molecules [78]. The latter is important for improving the SEOP efficiency and for decreasing the decay rate of the noble-gas spins due to the molecular interaction. The alkali spins are maintained at a constant $p_a = 90\%$ by continuous optical-pumping and experience a destruction rate $\gamma_s = 6800 \text{ s}^{-1}$ with the pump beam present. The ^{129}Xe atoms are polarized via SEOP to $p_b = 65\%$, lim-

ited by relaxation due to collisions with the alkali yielding $\gamma_k = 0.044 \text{ s}^{-1}$. It is possible to decrease γ_k during the memory time by lowering the alkali density. This configuration has $J = 580 \text{ s}^{-1}$ and, for $C = 100$ and $\gamma_\Omega = 15\gamma_s$, gives $\gamma_J = 3.2 \text{ s}^{-1}$ and an efficiency of $\eta_{\text{tot}} = 86\%$ for the adiabatic scheme. Note that $J < \gamma_s$, so that the scheme is only suitable for an adiabatic operation.

B. Low buffer-gas pressure

For the low-pressure configurations, we consider a Cs- ^{129}Xe mixture enclosed in a cylindrical cell with anti-relaxation coating. The alkali spins decohere by binary collisions with other alkali atoms, by three-body collisions with xenon atoms, and by interaction with the cell walls. The three-body collisions are associated with the formation of short-lived Cs- ^{129}Xe (Van-der-Waals) molecules, which limit the attainable degree of polarization p_a and significantly increase the destruction rate γ_s . To mitigate this process, we decrease the molecular formation rate by considering a relatively low density $n_b = 7 \times 10^{15} \text{ cm}^{-3}$ of ^{129}Xe (0.2 Torr). At this pressure, the molecular formation rate per alkali atom $R_3 = Zn_b^2 \approx 2.5 \text{ s}^{-1}$ is comparable to the binary spin-exchange collision rate $R_2 = k_{\text{SE}}n_b$, where $Z = 5.3 \times 10^{-32} \text{ cm}^6\text{s}^{-1}$ [79] and $k_{\text{SE}} = 4.1 \times 10^{-16} \text{ cm}^3\text{s}^{-1}$ [60]. Here we consider two configurations based on different wall coatings, all compatible with the adiabatic mapping scheme as $J < \gamma_s$.

Paraffin coating. — Paraffin coating allows for $N_e \geq 1000$ bounces before spin randomization [80]. We consider a cylindrical cell of length $L = 3 \text{ cm}$ and radius $r = 1 \text{ cm}$. The alkali density is $n_a = 2 \times 10^{12} \text{ cm}^{-3}$ (temperature 70°C), and $\gamma_s = 85 \text{ s}^{-1}$ due to collisions with

the walls and the background xenon. To allow for operation in the adiabatic regime for a duration longer than the alkali-spin lifetimes, an alkali-spin polarization of $p_a = 90\%$ is maintained by continuous optical-pumping [80–83]. While standard optical pumping would typically increase the relaxation rate in the dark by a factor of $p_a/(1 - p_a)$, pumping of the lower hyperfine manifold facilitated by spin-exchange collisions allows for efficient pumping of the upper manifold with reduced spin at the upper manifold. Under these conditions, the noble-gas spin polarization is maintained at $p_b = 50\%$ via binary and molecular spin-exchange collisions assuming a coherence time of $\gamma_k^{-1} = 9$ minutes limited by collisions with alkali atoms. These parameters yield $J = 15 \text{ s}^{-1}$ and $C = 60$ for a cavity with a finesse $\mathcal{F} = 5$. Here mapping of the optical signal onto the orientation moment of the alkali spins can be implemented in any standard mapping scheme, such as EIT of linearly polarized light tuned to the $F = 4 \rightarrow F = 3$ optical transition of the D1 line [35]. For $\gamma_\Omega = 15\gamma_s$, we get $\gamma_J = 0.17 \text{ s}^{-1}$ and a memory efficiency of $\eta_{\text{tot}} = 85\%$.

Alkane coating.— A configuration based on alkane coating could allow $N_e = 10^5$ wall bounces before spin randomization [80, 84]. We consider an cesium vapor density of $n_a = 9 \times 10^{12} \text{ cm}^{-3}$ (temperature 90°C) in a narrow cylindrical cell with $L = 2 \text{ cm}$ and $r = 1 \text{ mm}$ to mitigate radiation trapping. Maintaining $p_a = 90\%$ by continuous optical-pumping of the lower hyperfine manifold, yields $p_b = 50\%$, $\gamma_s = 50 \text{ s}^{-1}$, $\gamma_k^{-1} = 140 \text{ s}$, $J = 29 \text{ s}^{-1}$, and $C = 100$ (cavity finesse $\mathcal{F} \sim 2$). For $\gamma_\Omega = 50\gamma_s$, we get $\gamma_J = 0.35 \text{ s}^{-1}$ and a memory efficiency of $\eta_{\text{tot}} = 94\%$.

X. SUMMARY AND DISCUSSION

The theory presented in this work sets the ground for utilizing noble-gas spins as a quantum memory for light. The presented solutions enable efficient storage of non-classical states of light for unprecedented storage times. We outline various feasible experimental configurations, demonstrating how such memories could be designed and realized.

It is interesting to examine the role of δ_s particularly in the adiabatic regime. Since the alkali spin \hat{S} acts as a mediator, δ_s plays a similar role to the one-photon detuning Δ in standard alkali-only memories operating with adiabatic $\hat{\mathcal{P}}$. Working near the compensation point ($\delta_s \ll J, \gamma_s$) is equivalent to an on-resonance operation of spin memories (such as EIT). High efficiency however can also be realized far from compensation ($\delta_s \gg J, \gamma_s$), similar to operation of off-resonant memories (so-called Raman storage [23]).

We also note that imperfect polarization $p_b < 1$ of the noble-gas spins reduces the coupling rate $J \propto \sqrt{p_b}$ and increases the initial (incoherent) excitation of the collec-

tive mode $\langle \hat{\mathcal{K}}^\dagger \hat{\mathcal{K}} \rangle_0 = 1 - p_b > 0$. The latter could lead to readout and emission of a noise photon with probability $1 - p_b$, reducing the fidelity of the memory when storing single photons. However, this noise photon can potentially be read out prior to the storage process, via the same spin-exchange mechanism and retrieval procedure used for reading out the signal photon, leaving $\langle \hat{\mathcal{K}}^\dagger \hat{\mathcal{K}} \rangle_0 = 0$. The rate at which the collective mode is replenished with incoherent excitation is γ_k , leaving ample time for the storage and retrieval of the signal photon. In fact, the read-out of the noise happens naturally in the sequential mapping process (strong-coupling regime $J \gg \gamma_s$), as the transfer process $\hat{S} \rightarrow \hat{\mathcal{K}}$ is bi-directional and accompanied by the reverse transfer $\hat{\mathcal{K}} \rightarrow \hat{S}$. We shall explore these possibilities in a future publication. Furthermore, the initial incoherent excitations are insignificant for squeezed-state storage. An ensemble of spin-1/2 particles satisfies $\langle \hat{\mathcal{K}}^\dagger \hat{\mathcal{K}} + \hat{\mathcal{K}} \hat{\mathcal{K}}^\dagger \rangle = 1$, and therefore the two quadratures of the collective mode $(\hat{\mathcal{K}} \pm \hat{\mathcal{K}}^\dagger)/\sqrt{2}$ maintain vacuum properties [17, 58]. Squeezed states comprise a large number of photons and are therefore resilient to this noise.

The presented model is not limited to noble-gas spin systems and could be applied to analyze quantum memories in other four-level systems. These include, for example, an atomic system with a ladder of excited electronic orbitals [85–87]. Other hybrid systems with both optically accessible and inaccessible spins, such as quantum dots, diamond color-centers, and rare-earth impurities interacting with nearby nuclear spins in the crystal, are of much current interest. Unlike the case of noble-gas spins, where J can only be varied very slowly, these systems could have controllable $J(t)$ and benefit from the operation of $\hat{\mathcal{P}}$ outside the adiabatic regime, potentially going beyond the presented solutions.

O.K., R.S., E.R., and O.F. acknowledge financial support by the Israel Science Foundation, the European Research Council starting investigator grant Q-PHOTONICS 678674, the Pazy Foundation, the Minerva Foundation with funding from the Federal German Ministry for Education and Research, and the Laboratory in Memory of Leon and Blacky Broder. A.V.G. acknowledges support by ARL CDQI, ARO MURI, NSF PFC at JQI, AFOSR, AFOSR MURI, DoE BES Materials and Chemical Sciences Research for Quantum Information Science program (award No. DE-SC0019449), DoE ASCR FAR-QC (award No. DE-SC0020312), DoE ASCR Quantum Testbed Pathfinder program (award No. DE-SC0019040), and NSF PFCQC program.

Appendix A: Heisenberg-Bloch-Langevin equations

The explicit form of the Heisenberg-Bloch-Langevin equations for $\hat{\sigma}_{\mu\nu}(\mathbf{r}, t)$ is obtained by substituting \mathcal{H} from

Eqs. (13) and (17) into Eq. (19), yielding

$$\begin{aligned} \partial_t \hat{\sigma}_{\downarrow p} &= -[\gamma_p + i\Delta - i\frac{[I]}{4}\zeta(\hat{\sigma}_{\downarrow\downarrow} - \hat{\sigma}_{\uparrow\uparrow})]\hat{\sigma}_{\downarrow p} \\ &+ i\Omega(\mathbf{r}, t)\hat{\sigma}_{\downarrow\uparrow} + ig(\mathbf{r})(\hat{\sigma}_{\downarrow\downarrow} - \hat{\sigma}_{pp})\hat{\mathcal{E}} \\ &+ i\frac{\sqrt{[I]}}{2}\zeta\hat{\sigma}_{\uparrow p}\hat{\sigma}_{\downarrow\uparrow} + D_a\nabla^2\hat{\sigma}_{\downarrow p} + \hat{f}_{\downarrow p}, \end{aligned} \quad (\text{A1})$$

$$\begin{aligned} \partial_t \hat{\sigma}_{\downarrow\uparrow} &= -[\gamma_s + i\delta_s + i\frac{qI-1}{4}[I]\zeta(\sigma_{\downarrow\downarrow} - \sigma_{\uparrow\uparrow})]\hat{\sigma}_{\downarrow\uparrow} \\ &+ i\Omega^*(\mathbf{r}, t)\hat{\sigma}_{\downarrow p} - i\frac{\sqrt{[I]}}{2}\zeta(\hat{\sigma}_{\downarrow\downarrow} - \hat{\sigma}_{\uparrow\uparrow})\hat{\sigma}_{\downarrow\uparrow} \\ &- ig(\mathbf{r})\hat{\sigma}_{p\uparrow}\hat{\mathcal{E}} + D_a\nabla^2\hat{\sigma}_{\downarrow\uparrow} + \hat{f}_{\downarrow\uparrow}, \end{aligned} \quad (\text{A2})$$

$$\begin{aligned} \partial_t \hat{\sigma}_{\downarrow\uparrow} &= -[\gamma_k + i\delta_k - i\frac{[I]}{2}\zeta(\hat{\sigma}_{\downarrow\downarrow} + qI\hat{\sigma}_{\uparrow\uparrow})]\hat{\sigma}_{\downarrow\uparrow} \\ &- i\frac{\sqrt{[I]}}{2}\zeta\hat{\sigma}_{\downarrow\uparrow}(\hat{\sigma}_{\downarrow\downarrow} - \hat{\sigma}_{\uparrow\uparrow}) + D_b\nabla^2\hat{\sigma}_{\downarrow\uparrow} + \hat{f}_{\downarrow\uparrow}, \end{aligned} \quad (\text{A3})$$

where $\gamma_p \equiv \gamma_{\downarrow p}$, $\gamma_s \equiv \gamma_{\downarrow\uparrow}$, and $\gamma_k \equiv \gamma_{\downarrow\uparrow}$. These operators satisfy the commutation relations of continuous spin operators

$$\begin{aligned} [\hat{\sigma}_{\mu\nu}(\mathbf{r}, t), \hat{\sigma}_{\alpha\beta}(\mathbf{r}', t)] &= \\ &= \delta(\mathbf{r} - \mathbf{r}')(\delta_{\alpha\nu}\hat{\sigma}_{\mu\beta}(\mathbf{r}, t) - \delta_{\beta\mu}\hat{\sigma}_{\alpha\nu}(\mathbf{r}, t)). \end{aligned} \quad (\text{A4})$$

The equations can be further simplified by using the following assumptions: the excited state is unpopulated, $\hat{\sigma}_{pp} \approx 0$ if the control power is kept low ($\Omega \ll \gamma_{\downarrow p}$); $\hat{\sigma}_{p\uparrow} \approx 0$ for weak input pulses $\langle \hat{\mathcal{E}}^\dagger \hat{\mathcal{E}} \rangle \ll (\Omega/g)^2$; the collective operator $\hat{\sigma}_{\downarrow\downarrow} \approx p_a n_a$ is determined by the density of alkali atoms n_a and by the degree of ground-state polarization p_a , which is kept high via optical pumping $p_a \rightarrow 1$, such that $\hat{\sigma}_{\uparrow\uparrow} \approx 0$; and similarly the collective operator $\hat{\sigma}_{\downarrow\uparrow} \approx p_b n_b$ is determined by the density of noble-gas atoms n_b and by the degree of polarization p_b , which satisfies $p_b \lesssim 1$ owing to spin-exchange optical pumping (SEOP). We also note that the collisional shift and the diffusion terms have negligible effect on the optical linewidth. The simplified equations of motion are then given by

$$\begin{aligned} \partial_t \hat{\sigma}_{\downarrow p} &= -(\gamma_p + i\Delta)\hat{\sigma}_{\downarrow p} + i\Omega(\mathbf{r}, t)\hat{\sigma}_{\downarrow\uparrow} \\ &+ iG(\vec{r})\hat{\mathcal{E}} + \hat{f}_{\downarrow p}, \end{aligned} \quad (\text{A5})$$

$$\begin{aligned} \partial_t \hat{\sigma}_{\downarrow\uparrow} &= -(\gamma_s + i\delta_s - D_a\nabla^2)\hat{\sigma}_{\downarrow\uparrow} + i\Omega^*(\mathbf{r}, t)\hat{\sigma}_{\downarrow p} \\ &- i(\zeta\sqrt{[I]}p_a n_a/2)\hat{\sigma}_{\downarrow\uparrow} + \hat{f}_{\downarrow\uparrow}, \end{aligned} \quad (\text{A6})$$

$$\begin{aligned} \partial_t \hat{\sigma}_{\downarrow\uparrow} &= -(\gamma_k + i\delta_k - D_b\nabla^2)\hat{\sigma}_{\downarrow\uparrow} \\ &- i(\zeta\sqrt{[I]}p_b n_b/2)\hat{\sigma}_{\downarrow\uparrow} + \hat{f}_{\downarrow\uparrow}, \end{aligned} \quad (\text{A7})$$

where $\Delta \rightarrow \Delta - \frac{[I]}{4}\zeta p_b n_b$. The modified detuning of the alkali spins $\delta_s = \delta_s + (qI - 1)[I]\zeta n_b p_b/4$ accounts for the collisional shift that the alkali spins experience due to the magnetized noble-gas spins. Similarly, the modified detuning of the noble-gas spins $\delta_k = \delta_k - [I]\zeta p_a n_a/2$ accounts for the collisional shift that the noble-gas spins experience due to the magnetized alkali spins.

Appendix B: Properties of the Quantum Noise

In this appendix, we present the properties of the quantum noise operators. In the Heisenberg-Langevin picture, the relaxation of the quantum operators is accompanied by stochastic quantum noise [64]. In our model, we assume that the noise operators $\hat{f}_{\mu\nu}(\mathbf{r}, t)$ defined in Eq. (19) are temporally white, satisfying

$$\langle \hat{f}_{\mu\nu}(\mathbf{r}, t) \rangle = 0 \quad (\text{B1})$$

with variance

$$\begin{aligned} \langle \hat{f}_{\mu\nu}(\mathbf{r}, t)\hat{f}_{\alpha\beta}(\mathbf{r}', t') \rangle &= C_{\mu\nu\alpha\beta}(\mathbf{r}, \mathbf{r}')\delta(t - t') \\ &+ \delta_{\nu\alpha}(\gamma_{\mu\nu} + \gamma_{\nu\beta} - \gamma_{\mu\beta})\sigma_{\mu\beta}(\mathbf{r}, t)\delta(\mathbf{r} - \mathbf{r}')\delta(t - t'), \end{aligned} \quad (\text{B2})$$

where $C_{\mu\nu\alpha\beta}(\mathbf{r}, \mathbf{r}')$ is the diffusion noise correlation function for operators $\hat{\sigma}_{\mu\nu}, \hat{\sigma}_{\alpha\beta}$. The noise operators are essential for preserving the commutation relations $[\hat{\sigma}_{\mu\nu}(\mathbf{r}, t), \hat{\sigma}_{\alpha\beta}(\mathbf{r}', t)]$.

For polarized spins, in the Holstein-Primakoff approximation, the operators $\hat{\mathcal{P}}(\mathbf{r}, t)$, $\hat{\mathcal{S}}(\mathbf{r}, t)$, and $\hat{\mathcal{K}}(\mathbf{r}, t)$ act as local bosonic annihilation operators. The noise terms $\hat{f}_{\mathcal{P}} = \hat{f}_{\downarrow p}/\sqrt{p_a n_a}$, $\hat{f}_{\mathcal{S}} = \hat{f}_{\downarrow\uparrow}/\sqrt{p_a n_a}$, and $\hat{f}_{\mathcal{K}}(\mathbf{r}, t) = \hat{f}_{\downarrow\uparrow}/\sqrt{p_b n_b}$, appearing in Eqs. (20)-(22), then act as vacuum noise operators satisfying

$$\langle \hat{f}_q(\mathbf{r}, t) \rangle = \langle \hat{f}_q^\dagger(\mathbf{r}, t)\hat{f}_q(\mathbf{r}', t') \rangle = 0 \quad (\text{B3})$$

and

$$\begin{aligned} [\hat{f}_q(\mathbf{r}, t), \hat{f}_q^\dagger(\mathbf{r}', t')] &= \langle \hat{f}_q(\mathbf{r}, t), \hat{f}_q^\dagger(\mathbf{r}', t') \rangle \\ &= 2(\gamma_q - D_q\nabla^2)\delta(\mathbf{r} - \mathbf{r}')\delta(t - t'). \end{aligned} \quad (\text{B4})$$

Here $q \in \{\mathcal{P}, \mathcal{S}, \mathcal{K}\}$, with $\gamma_{\mathcal{P}} \equiv \gamma_p$, $\gamma_{\mathcal{S}} \equiv \gamma_s$, $\gamma_{\mathcal{K}} \equiv \gamma_k$, $D_{\mathcal{P}} = D_{\mathcal{S}} \equiv D_a$, and $D_{\mathcal{K}} \equiv D_b$. The first term in Eq. (B4) describes a spatially-white noise with variance $2\gamma_q$, which is associated with the relaxation rate γ_q via the fluctuation-dissipation relations. The second term is the diffusion component of the noise correlation function, independent of the other relaxation mechanisms incorporated in γ_q [63]. The diffusion-induced decoherence rate of $\hat{\mathcal{P}}$ is negligible compared to γ_p and so is the contribution of diffusion to the excited state noise.

Appendix C: Spatial modes representation

Here we present the decomposition of the spin operators into spatial mode functions and various choices for these functions. Equations (21) and (22) contain non-local terms due to atomic diffusion. Consequently, the evolution of the spin operators is better described using a decomposition into multiple nonlocal (spatial) modes. We therefore write $\hat{\mathcal{P}}(\mathbf{r}, t) = \sum_i u_i^{(p)}(\mathbf{r})\hat{\mathcal{P}}_i(t)$, $\hat{\mathcal{S}}(\mathbf{r}, t) = \sum_m u_m^{(s)}(\mathbf{r})\hat{\mathcal{S}}_m(t)$, and $\hat{\mathcal{K}}(\mathbf{r}, t) = \sum_n u_n^{(k)}(\mathbf{r})\hat{\mathcal{K}}_n(t)$, where each set of mode functions (u_p, u_s, u_k) is complete [17].

1. Optical dipole $\hat{\mathcal{P}}$

The optical dipole component that interacts with the field of the cavity in Eq. (25) is defined by the spatial overlap with the signal

$$\hat{\mathcal{P}}(t) = \sqrt{\frac{V_{\text{cav}}}{V}} \int_V f_{\varepsilon}^*(\mathbf{r}) \hat{\mathcal{P}}(\mathbf{r}, t) d^3\mathbf{r}. \quad (\text{C1})$$

It is therefore fruitful to choose the set of modes $u_i^{(p)}(\mathbf{r})$ in which a specific mode $u_0^{(p)}(\mathbf{r})$ maximizes that integral, and all other modes are orthogonal. We thus choose $u_0^{(p)}(\mathbf{r} \in \mathbf{V}) = \sqrt{V_{\text{cav}}/V} f_{\varepsilon}(\mathbf{r})$ [and $u_0^{(p)}(\mathbf{r} \notin \mathbf{V}) = 0$] and obtain $\hat{\mathcal{P}}(t)$ by substituting Eq. (28) into Eq. (C1),

$$\hat{\mathcal{P}}(t) = i \frac{\Omega(t) \sum_m b_m \hat{\mathcal{S}}_m(t) + \sqrt{2\gamma_p C} \hat{\mathcal{E}}_{\text{in}}(t) - i \hat{f}_{\mathcal{P}}}{\gamma_p (C + 1) + i\Delta}. \quad (\text{C2})$$

The optical mode-matching parameter b_m is given by

$$b_m = \sqrt{V_{\text{cav}}} \int_V u_m^{(s)}(\mathbf{r}) u_0^{(p)*}(\mathbf{r}) f_c(\mathbf{r}) d^3\mathbf{r}, \quad (\text{C3})$$

characterizing the spatial overlap of the alkali-spin modes $u_m^{(s)}(\mathbf{r})$ with the mode $u_0^{(p)}(\mathbf{r})$ of the optical dipole, weighted by the mode function of the optical control field in the cavity $\sqrt{V_{\text{cav}}} f_c(\mathbf{r})$. The condition $\sum_m |b_m|^2 \leq 1$ is satisfied. We also define the noise operator of the single excited mode by $\hat{f}_{\mathcal{P}}(t) = \int_V u_0^{(p)*}(\mathbf{r}) \hat{f}_{\mathcal{P}}(\mathbf{r}, t) d^3\mathbf{r}$.

Correspondingly, Eq. (25) is transformed to

$$\hat{\mathcal{E}}_{\text{out}}(t) = \alpha \hat{\mathcal{E}}_{\text{in}} - \sum_m p_{\text{out}}^{(m)}(t) \hat{\mathcal{S}}_m + \hat{f}_{\mathcal{E}}, \quad (\text{C4})$$

where we define

$$\alpha = \frac{\gamma_p (1 - C) + i\Delta}{\gamma_p (1 + C) + i\Delta}, \quad (\text{C5})$$

the coefficients $p_{\text{out}}^{(m)}(t) = Q b_m \Omega(t)$, and the additional noise operator for the output field $\hat{f}_{\mathcal{E}} = Q \hat{f}_{\mathcal{P}}$, where Q is defined in Eq. (33).

2. Noble-gas spin $\hat{\mathcal{K}}$

The natural choice of mode functions for the collective noble-gas spin is the set of eigenmodes of the diffusion-relaxation operator [63]

$$(\gamma_k - D_b \nabla^2) u_n^{(k)}(\mathbf{r}) = \gamma_n^{(k)} u_n^{(k)}(\mathbf{r}), \quad (\text{C6})$$

assuming nondestructive (Neumann) boundary conditions. Here $\gamma_n^{(k)}$ represents the relaxation rate of the n^{th} mode. Using these mode functions, the equations of motion of the noble-gas spin can be written as

$$\partial_t \hat{\mathcal{K}}_n = -(\gamma_n^{(k)} + i\delta_k) \hat{\mathcal{K}}_n - iJ \sum_m c_{mn}^* \hat{\mathcal{S}}_m + \hat{f}_{\mathcal{K}}^{(n)}, \quad (\text{C7})$$

where

$$c_{mn} = \int_V u_m^{(s)*}(\mathbf{r}) u_n^{(k)}(\mathbf{r}) d^3\mathbf{r} \quad (\text{C8})$$

describes the matching of the noble-gas spin modes to the alkali-spin modes [57]. The matrix $[c_{mn}]$ is unitary, satisfying $\sum_n c_{mn}^* c_{nj} = \delta_{mj}$. The normalized noise operators of the spin modes are $\hat{f}_{\mathcal{K}}^{(n)} = \int_V u_n^{(k)*}(\mathbf{r}) \hat{f}_{\mathcal{K}}(\mathbf{r}, t) d^3\mathbf{r}$. In particular, the $n = 0$ mode is the uniform spin mode, $u_0^{(k)}(\mathbf{r}) = 1/\sqrt{V}$, unaffected by diffusion and exhibiting a minimal decay at a rate $\gamma_k = \gamma_0^{(k)}$. This mode is utilized here as the single mode of the long-lived quantum memory

$$\hat{\mathcal{K}}(t) \equiv \hat{\mathcal{K}}_0(t) = \frac{1}{\sqrt{V}} \int \hat{\mathcal{K}}(\mathbf{r}, t) d^3\mathbf{r}. \quad (\text{C9})$$

3. Alkali spin $\hat{\mathcal{S}}$

Before choosing a particular basis for the alkali spins, we first write Eq. (21) for a general basis $u_m^{(s)}$. Using Eq. (C2), we obtain

$$\begin{aligned} \partial_t \hat{\mathcal{S}}_m &= -(\gamma_s + i\delta_s) \hat{\mathcal{S}}_m - \sum_j (\Gamma_{\Omega} b_m^* b_j + d_{mj}) \hat{\mathcal{S}}_j \\ &\quad - iJ \sum_n c_{mn} \hat{\mathcal{K}}_n - p_{\text{in}}^{(m)}(t) \hat{\mathcal{E}}_{\text{in}} + \hat{F}_{\mathcal{S}}^{(m)}, \end{aligned} \quad (\text{C10})$$

Generally, the modes $u_m^{(s)}$ are coupled by the atomic diffusion, as represented by the coefficients

$$d_{mj} = -D_a \int_V d^3\mathbf{r} u_m^{(s)*}(\mathbf{r}) \nabla^2 u_j^{(s)}(\mathbf{r}). \quad (\text{C11})$$

The coefficients $p_{\text{in}}^{(m)}(t) = Q b_m^* \Omega^*(t)$ describe the coupling of each alkali-spin mode to the input light field. The normalized noise operators of the alkali spin are $\hat{F}_{\mathcal{S}}^{(m)} = \int_V u_m^{(s)*}(\mathbf{r}) \hat{f}_{\mathcal{S}}(\mathbf{r}, t) d^3\mathbf{r} + i p_{\text{in}}^{(m)} \hat{f}_{\mathcal{P}} / \sqrt{2C\gamma_p}$, including the quantum noise associated with the control beam (light-induced relaxation).

To choose a mode-function basis for the alkali spins, we examine eigenvalues of the matrix $[\gamma_s \delta_{mj} + \gamma_{\Omega} b_m^* b_j + d_{mj}]$, which correspond to the relaxation rates of the modes $\gamma_m^{(s)}$. It follows that a convenient choice of mode basis exists in two limiting regimes: when the dynamics is dominated by diffusion (*e.g.*, in the dark $\gamma_{\Omega} \ll D_a/V^{2/3}$) and $[d_{mj}]$ is diagonal, or when the dynamics is dominated by power broadening ($\gamma_{\Omega} \gg D_a/V^{2/3}$) and $[b_m^* b_j]$ is diagonal. Here we consider these two regimes.

a. Diffusion-dominated regime

In the regime $\gamma_{\Omega} \ll D_a/V^{2/3}$, the diffusion dominates over power broadening. The natural choice of basis is the

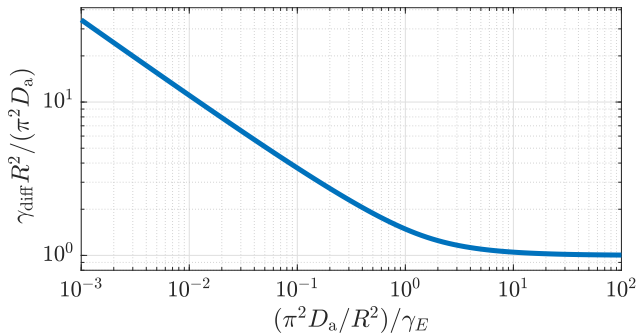


Figure 8. Effective diffusion-induced decay rate of the uniform mode of alkali spins as a function of the coupling duration $1/\gamma_E$.

set of eigenmodes of the diffusion-relaxation operator for the alkali-metal spins

$$(\gamma_s - D_a \nabla^2) u_m^{(s)}(\mathbf{r}) = \gamma_m^{(s)} u_m^{(s)}(\mathbf{r}), \quad (\text{C12})$$

satisfying destructive (Dirichlet) or partially-destructive (Robin) boundary condition, depending on the quality of the anti-relaxation coating of the cell walls [60, 63]. This set of mode functions best applies for the sequential mapping strategy in section VI and Appendix H. In Appendix D, we calculate the values of b_m and c_{mn} for an uncoated spherical cell.

b. Light-dominated regime

In the regime $\gamma_\Omega \gg D_a/V^{2/3}$, power broadening due to the control beam dominates over diffusion. It is then possible to engineer the spatial profile of the control field such that the $m = 0$ spin mode becomes the uniform mode $u_0^{(s)}(\mathbf{r}) = 1/\sqrt{V}$, and $b_m = \delta_{m0}$. This can be realized by maintaining the term $f_c(\mathbf{r})f_\varepsilon^*(\mathbf{r})$ constant within the atomic cell, such that the term $\Omega^*(\mathbf{r}, t)\hat{\mathcal{P}}(\mathbf{r}, t)$ appearing in Eq. (21) is spatially independent. This in turn yields a uniform two-photon excitation of the alkali spin ensemble.

To exemplify this, in the large cavity limit, the spatial modes are approximately the free-space modes $f_c(\mathbf{r}) \approx e^{i\mathbf{k}_c \cdot \mathbf{r}}/\sqrt{V_{\text{cav}}}$ and $f_\varepsilon^*(\mathbf{r}) = e^{-i\mathbf{k}_\varepsilon \cdot \mathbf{r}}/\sqrt{V_{\text{cav}}}$. For an enclosure of length L , if $|\mathbf{k}_\varepsilon - \mathbf{k}_c|L \ll 1$, then $f_c(\mathbf{r})f_\varepsilon^*(\mathbf{r}) \approx 1/V_{\text{cav}}$ and the input signal excites the uniform spin mode efficiently. This condition is often satisfied in experiments when the signal and control fields are nearly degenerate. Under these conditions, we get $b_0 = c_{10}^* = 1$ while $b_m = c_{m0}^* = 0$ for $m \neq 1$. We can then approximate the dynamics in Eq. (31) with the use of the uniform spin operator

$$\hat{S}(t) \equiv \frac{1}{\sqrt{V}} \int_V \hat{S}(\mathbf{r}, t) d^3\mathbf{r}. \quad (\text{C13})$$

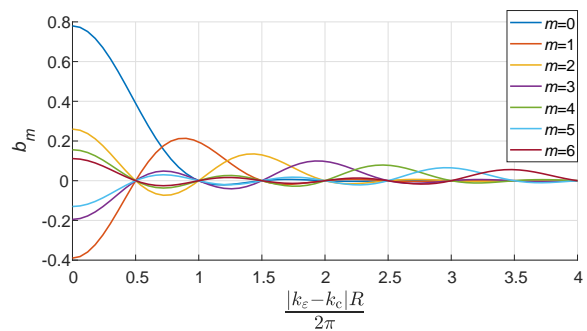


Figure 9. Mode overlap of the uniform spin distribution with the signal and control fields in the cavity, cf. Eq. (C3), for the first seven modes. The condition $|\mathbf{k}_\varepsilon - \mathbf{k}_c|R \ll 1$ is typically satisfied.

To account for the contribution of higher spatial modes in Eq. (C10), we approximate the multi-exponential decay using a single effective rate

$$\gamma_s \rightarrow \gamma_s + \gamma_{\text{diff}}. \quad (\text{C14})$$

While for the sequential scheme it is natural to decompose the uniform spin mode into the diffusion eigenmodes, which lead to a multi-exponential decay [cf. Eqs. (H1)-(H2)], for the adiabatic scheme the dynamics can be well approximated by a single exponential decay, since γ_Ω dominates over the diffusion rate of the least decaying modes. We therefore use Eq. (31), which neglects the contribution of the other spatial modes to the uniform alkali mode. To best approximate the dynamics and the diffusion-induced relaxation in Eq. (C14), we define the effective rate

$$\gamma_{\text{diff}} = -\gamma_E \ln \left[\sum_{m=0}^{\infty} |c_{m0}|^2 \exp\left(\frac{\gamma_\Omega + \gamma_s - \gamma_m^{(s)}}{\gamma_E}\right) \right], \quad (\text{C15})$$

which weighs the contribution of the different diffusion modes within some coupling duration $1/\gamma_E$. In Fig. 8, we present the diffusion decay rate γ_{diff} in an uncoated cell with respect to the decay rate $D_a\pi^2/R^2$ of the lowest-order diffusion mode. In the calculations presented in the main text, we choose $\gamma_E = \gamma_\Omega + \gamma_s$, such that γ_{diff} approaches $D_a\pi^2/R^2$.

Appendix D: Numerical evaluation of the spatial mode decomposition for a spherical cell

In this appendix, we present a numerical evaluation of the overlap coefficients b and c and derive an approximate expression for the diffusion relaxation of the uniform alkali-spin mode. We consider a spherical cell of radius R and define the diffusion modes following Ref. [63]. In a spherical cell, the diffusion modes are labeled by (m, ℓ, μ) , where m characterizes the radial dependence, and (ℓ, μ)

mode number (m)	$\frac{\gamma_m^{(s)} - \gamma_s}{D_a \pi^2 / R^2}$	$\frac{\gamma_m^{(k)} - \gamma_k}{D_b \pi^2 / R^2}$
0	1	0
1	4	2.05
2	9	6.05
3	16	12.05
4	25	20.05
5	36	30.05
6	49	42.05

Table II. Diffusion-induced decay rates for the first seven spherically symmetric modes of alkali spins ($\gamma_m^{(s)} - \gamma_s$) and noble-gas spins ($\gamma_m^{(k)} - \gamma_k$) in an uncoated spherical cell [cf. Eqs. (C6) and (C12)].

represent the angular symmetry. Since we ultimately consider storage on the noble-gas uniform mode, we use only the spherically-symmetric modes, *i.e.* $\ell = \mu = 0$. We therefore use a single label m to index the modes.

1. Representation of b

We calculate the overlap b_m between the alkali spin and the optical field, as defined in Eq. (C3). We set the $\hat{\mathbf{z}}$ axis as the cavity axis, such that for the control we have $f_c(\mathbf{r}) = e^{-ik_c z} / \sqrt{V_{\text{cav}}}$, and the optical dipole spatially follows the signal field $u_0^{(p)*}(\mathbf{r}) = e^{ik_\varepsilon \cdot \mathbf{r}} / \sqrt{V}$. With these, we get for the spherically-symmetric modes

$$b_m = \int_0^R r^2 dr \int_0^\pi \sin \theta d\theta \int_0^{2\pi} b_m(r, \theta, \varphi) d\varphi, \quad (\text{D1})$$

where

$$b_m(r, \theta, \varphi) = \frac{\sqrt{3} j_0(\pi x_m r / R) \cdot e^{i(k_\varepsilon - k_c)z}}{A_m 4\pi R^3}. \quad (\text{D2})$$

Here $j_0(x)$ denotes the zeroth-order spherical Bessel function, πx_m is its m^{th} root such that $j_0(\pi x_m) = 0$, and A_m is the normalization factor defined as

$$A_m^2 R^3 = \int_0^R r^2 j_0^2(\pi x_m r / R) dr. \quad (\text{D3})$$

Expanding the expression $\exp(i(k_\varepsilon - k_c)z)$ as a series of Bessel functions yields

$$b_m = \frac{\sqrt{3}}{A_m} \int_0^1 \xi^2 j_0(\pi x_m \xi) \left[J_0((k_\varepsilon - k_c)R\xi) + 2 \sum_{\kappa=1}^{\infty} \frac{(-1)^\kappa J_{2\kappa}((k_\varepsilon - k_c)R\xi)}{1 - 4\kappa^2} \right] d\xi. \quad (\text{D4})$$

In Fig. 9, we present b_m for the first seven modes $m = 0, \dots, 6$. For standard alkali-spin memories, the condition $|k_\varepsilon - k_c|R \ll 1$ is typically satisfied, yielding the identity $b_m = c_{m0}$.

	$n = 0$	$n = 1$	$n = 2$	$n = 3$	$n = 4$	$n = 5$	$n = 6$
$m = 0$	0.780	0.609	-0.126	0.058	-0.033	0.022	-0.016
$m = 1$	-0.390	0.652	0.622	-0.158	0.079	-0.049	0.033
$m = 2$	0.260	-0.275	0.0647	0.0627	-0.173	0.091	-0.058
$m = 3$	-0.195	0.182	-0.256	0.644	0.629	-0.181	0.098
$m = 4$	0.156	-0.139	0.168	-0.246	0.643	0.631	-0.187
$m = 5$	-0.130	0.112	-0.128	0.159	-0.239	0.642	0.632
$m = 6$	0.111	-0.095	0.104	-0.121	0.154	-0.235	0.641

Table III. The overlap coefficients c_{mn} between the m^{th} diffusion eigenmode of alkali spins and the n^{th} diffusion eigenmode of noble-gas spins in an uncoated cell [cf. Eq. (C8)].

2. Representation of c

In an uncoated cell, the alkali and noble-gas spins interact differently with the surface of the glass wall, leading to different boundary conditions for the diffusion of spins (Neumann for noble-gas spins and Dirichlet for alkali spins) [63]. This in turn leads to different sets of radial eigenmodes of the two spin species in a spherical cell. Under these conditions, we calculate the diffusion-induced decay rates $\gamma_m^{(s)} - \gamma_s$ for the alkali spins and $\gamma_n^{(k)} - \gamma_k$ for the noble-gas spins (see Table II) and the overlap coefficients for the modes of the two species c_{mn} (see Table III).

Appendix E: Conservation of excitations

Here we identify an integral relation, which can be viewed as a conservation law for the excitations. The excitations in the optical signal $\hat{\mathcal{E}}_{\text{in}}$ can be exchanged between the spin operators $\hat{\mathcal{P}}$, $\hat{\mathcal{S}}$, $\hat{\mathcal{K}}$, and finally be transferred to $\hat{\mathcal{E}}_{\text{out}}$. Using Eqs. (30), (31), and (34), we write the relation

$$\begin{aligned} & \langle \hat{\mathcal{E}}_{\text{out}}^\dagger \hat{\mathcal{E}}_{\text{out}} \rangle - \langle \hat{\mathcal{E}}_{\text{in}}^\dagger \hat{\mathcal{E}}_{\text{in}} \rangle + \partial_t (\langle \hat{\mathcal{P}}^\dagger \hat{\mathcal{P}} \rangle + \langle \hat{\mathcal{S}}^\dagger \hat{\mathcal{S}} \rangle + \langle \hat{\mathcal{K}}^\dagger \hat{\mathcal{K}} \rangle) \\ & = -2(\gamma_p \langle \hat{\mathcal{P}}^\dagger \hat{\mathcal{P}} \rangle + \gamma_s \langle \hat{\mathcal{S}}^\dagger \hat{\mathcal{S}} \rangle + \gamma_k \langle \hat{\mathcal{K}}^\dagger \hat{\mathcal{K}} \rangle). \end{aligned} \quad (\text{E1})$$

It is evident that, in a lossless cavity, excitations decay only through the relaxations γ_p , γ_s , and γ_k during the time that $\hat{\mathcal{P}}$, $\hat{\mathcal{S}}$, and $\hat{\mathcal{K}}$ are excited. Upon integration, we get the relation

$$\begin{aligned} & \int_{t_1}^{t_2} \langle \hat{\mathcal{E}}_{\text{out}}^\dagger \hat{\mathcal{E}}_{\text{out}} - \hat{\mathcal{E}}_{\text{in}}^\dagger \hat{\mathcal{E}}_{\text{in}} \rangle_t dt + \langle \hat{\mathcal{P}}^\dagger \hat{\mathcal{P}} \rangle_{t_2} - \langle \hat{\mathcal{P}}^\dagger \hat{\mathcal{P}} \rangle_{t_1} \\ & + \langle \hat{\mathcal{S}}^\dagger \hat{\mathcal{S}} \rangle_{t_2} - \langle \hat{\mathcal{S}}^\dagger \hat{\mathcal{S}} \rangle_{t_1} + \langle \hat{\mathcal{K}}^\dagger \hat{\mathcal{K}} \rangle_{t_2} - \langle \hat{\mathcal{K}}^\dagger \hat{\mathcal{K}} \rangle_{t_1} \\ & = -2 \int_{t_1}^{t_2} (\gamma_p \langle \hat{\mathcal{P}}^\dagger \hat{\mathcal{P}} \rangle_t + \gamma_s \langle \hat{\mathcal{S}}^\dagger \hat{\mathcal{S}} \rangle_t + \gamma_k \langle \hat{\mathcal{K}}^\dagger \hat{\mathcal{K}} \rangle_t) dt, \end{aligned} \quad (\text{E2})$$

which describes the conservation of excitations.

Appendix F: Storage and Retrieval of alkali memories

In this appendix, we review the formalism of Ref. [61] to describe storage and retrieval of optical memories using alkali spins.

Equation (31) is a linear stochastic differential equation for the alkali-spin operator. The solution for this equation is given by

$$\hat{S}(T) = \Phi_{T,-\infty} \hat{S}(-\infty) - \int_{-\infty}^T \Phi_{T,t} Q \Omega^* \hat{\mathcal{E}}_{\text{in}}(t) dt + \hat{\mathcal{W}}_S. \quad (\text{F1})$$

The first term describes the deterministic evolution of \hat{S} in the absence of an input signal. The second term describes the response of the spins to the input optical signal. The third term describes the stochastic response of the spin via the stochastic quantum process $\hat{\mathcal{W}}_S(T) = \int_{-\infty}^T \Phi_{T,\tau} \hat{F}_S(\tau) d\tau$. The operator $\Phi_{T,t}$ is the evolution in the interval $t < T$, given by

$$\Phi_{T,t} = \exp \left[- \int_t^T [\Gamma_\Omega(s) + \gamma_s + i\delta_s] ds \right]. \quad (\text{F2})$$

Note that this solution accounts for the diffusion-induced relaxation of the alkali spins in the power-broadened regime $\gamma_\Omega \gg D_a/V^{2/3}$ via Eqs. (C14) and (C15). We now focus on the storage and retrieval stages for $T = T'$.

Storage.— Initially $\langle \hat{S}^\dagger \hat{S} \rangle_{(t=-\infty)} = 0$, so the first term in Eq. (F1) vanishes. By defining the transfer function

$$h_\Omega(T, t) = -Q \Omega^* \Phi_{T,t}, \quad (\text{F3})$$

we write the alkali spin after storage as

$$\hat{S}(T) = \int_{-\infty}^T h_\Omega(T, t) \hat{\mathcal{E}}_{\text{in}}(t) dt + \hat{\mathcal{W}}_S(T). \quad (\text{F4})$$

The transfer function $h_\Omega(T, t)$ then satisfies

$$\int_{-\infty}^T e^{2\gamma_s(T-t)} |h_\Omega(T, t)|^2 dt \leq \sqrt{\frac{C+1}{C}}. \quad (\text{F5})$$

Maximal storage efficiency is realized by shaping the temporal profile of the control field $\Omega(t)$ to satisfy $h_\Omega(T, t) = A_\Omega \hat{\mathcal{E}}_{\text{in}}^*(t)$, where the normalization constant A_Ω is given by

$$A_\Omega = \sqrt{\frac{\int_{-\infty}^T |h_\Omega(T, s)|^2 ds}{\int_{-\infty}^T \langle \mathcal{E}_{\text{in}}^\dagger \mathcal{E}_{\text{in}} \rangle_s ds}}. \quad (\text{F6})$$

Using Eq. (F1), we can describe the storage efficiency for any input signal by

$$\eta_{\text{in}}^{(\mathcal{E} \rightarrow \mathcal{S})} = \frac{C}{C+1} \int_{-\infty}^T \langle \hat{\mathcal{E}}_{\text{in}}^\dagger \hat{\mathcal{E}}_{\text{in}} \rangle_t e^{2\gamma_s(t-T)} dt, \quad (\text{F7})$$

which approaches $C/(C+1)$ in the short pulse limit ($\gamma_s T \ll 1$), but otherwise depends on the temporal mode function of the input field.

Retrieval.— The output field during retrieval, obtained by substituting Eq. (30) in Eq. (29), is

$$\hat{\mathcal{E}}_{\text{out}}(t) = \alpha \hat{\mathcal{E}}_{\text{in}} - Q \Omega \hat{S} + \hat{f}_\mathcal{E}, \quad (\text{F8})$$

where α is given in Eq. (C5). Note that Eq. (F8) is the single-mode version of Eq. (C4). The output field squared for any $t \geq \tau + T$ is then given by

$$\langle \hat{\mathcal{E}}_{\text{out}}^\dagger \hat{\mathcal{E}}_{\text{out}} \rangle_t = |h_\Omega(t, \tau + T)|^2 \langle \hat{S}^\dagger \hat{S} \rangle_{(\tau+T)}, \quad (\text{F9})$$

assuming that $\hat{f}_\mathcal{E}$ satisfies vacuum properties and that $\langle \hat{\mathcal{E}}_{\text{in}}^\dagger \hat{\mathcal{E}}_{\text{in}} \rangle_{(t>T)} = 0$. The retrieval efficiency into some target temporal mode $f(t)$ is given by

$$\eta_{\text{out}}^{(\mathcal{S} \rightarrow \mathcal{E})} = \frac{C}{C+1} \frac{1}{\int_{\tau+T}^\infty |f(t)|^2 e^{2\gamma_s(t-\tau-T)} dt}, \quad (\text{F10})$$

where $f(t)$ is normalized such that $\int_{\tau+T}^\infty |f(t)|^2 dt = 1$. Like the storage efficiency, the retrieval efficiency approaches $C/(C+1)$ in the short pulse limit ($\gamma_s T \ll 1$), but otherwise depends on the desired temporal mode function of the output field.

Appendix G: Optimal δ_s

Here we analyze the dependence of the optimal storage schemes on δ_s . In the sequential scheme, in the first stage $\hat{\mathcal{E}}_{\text{in}} \rightarrow \hat{S}$, maximal storage efficiency is achieved when the integral in Eq. (F4) is maximized. Considering this integral as an inner product between the function h_Ω and $\mathcal{E}_{\text{in}}^*(t)$, we realize that maximal overlap appears for $h_\Omega(t) \propto \mathcal{E}_{\text{in}}^*(t)$ [61]. When both $\mathcal{E}_{\text{in}}(t)$ [Eq. (41)] and Ω are real and $\Delta = 0$, we obtain the condition

$$\text{Im}(h_\Omega(t)) = 0, \quad (\text{G1})$$

which is satisfied at any time for $\delta_s = 0$. In the second stage of the storage $\hat{S} \rightarrow \hat{\mathcal{K}}$, the exchange evolution depends on the exchange rate $\tilde{J}(\delta)$ [Eq. (57)], which in turn depends only on δ [cf. Eq. (56)], and is optimal for $\delta = 0$. Therefore, fixing $\delta_s = \delta_k = 0$ attains that optimum. We therefore conclude that the choice of $\delta_s = 0$ maximizes the efficiency.

In the adiabatic scheme, maximal storage efficiency is obtained when the integral in Eq. (70) is maximized. Considering this integral as an inner product, the maximum is now attained for $ih_J(t) \propto \mathcal{E}_{\text{in}}^*(t)$. For real $\mathcal{E}_{\text{in}}(t)$, Ω and for $\Delta = 0$, the condition is now

$$\text{Re}(h_J(t)) = 0. \quad (\text{G2})$$

Here δ_s takes the role of Δ in a standard Λ -system storage. Therefore, similarly, we can choose $\delta_s = 0$ and obtain the optimal solution with $\delta_k = 0$.

Appendix H: Multi mode description of the sequential mapping

In this appendix, we derive the solution for the multi-mode exchange evolution in the second stage $\hat{\mathcal{S}} \rightarrow \hat{\mathcal{K}}$ of the sequential mapping scheme. Using the diffusion eigenmodes for the alkali spins in Eq. (C12), the dynamics is described by

$$\partial_t \hat{\mathcal{S}}_m = -(\gamma_s^{(m)} + i\delta_s) \hat{\mathcal{S}}_m - iJ \sum_n c_{mn} \hat{\mathcal{K}}_n + \hat{f}_S^{(m)}, \quad (\text{H1})$$

$$\partial_t \hat{\mathcal{K}}_n = -(\gamma_k^{(n)} + i\delta_k) \hat{\mathcal{K}}_n - iJ \sum_m c_{mn}^* \hat{\mathcal{S}}_m + \hat{f}_K^{(n)}. \quad (\text{H2})$$

The spins experience coherent dynamics in the dark, with the alkali and noble-gas spin modes periodically exchanging excitations. The coefficients c_{mn} [Eq. (C8)] weigh the coupling of the m^{th} mode of one spin gas with the n^{th} mode of the other spin gas. The solution of Eqs. (H1-H2) reads

$$\begin{pmatrix} \hat{\mathcal{S}}(T') \\ \hat{\mathcal{K}}(T') \end{pmatrix} = \Psi_{T',T} \begin{pmatrix} \hat{\mathcal{S}}(T) \\ \hat{\mathcal{K}}(T) \end{pmatrix} + \begin{pmatrix} \hat{\mathcal{W}}_s(T') \\ \hat{\mathcal{W}}_k(T') \end{pmatrix}, \quad (\text{H3})$$

where the matrix $\Psi_{T',T}$ describes the evolution of the spins from time T to time T' , and the vector of stochastic operators is given by

$$\begin{pmatrix} \hat{\mathcal{W}}_s(T') \\ \hat{\mathcal{W}}_k(T') \end{pmatrix} = \int_T^{T'} \Psi_{T',t} \begin{pmatrix} \hat{f}_S(t) \\ \hat{f}_K(t) \end{pmatrix} dt. \quad (\text{H4})$$

For a constant magnetic field during the interaction, $\Psi_{T',T}$ is given by

$$\Psi_{T',T} = \exp \left[\begin{pmatrix} [A_s] & iJ[c] \\ iJ[c]^\dagger & [A_k] \end{pmatrix} (T' - T) \right], \quad (\text{H5})$$

where the matrices $[A_s]$, $[A_k]$, and $[c]$ have the elements $[A_s]_{mn} = (\gamma_s^{(m)} + i\delta_s) \delta_{mn}$, $[A_k]_{mn} = (\gamma_k^{(n)} + i\delta_k) \delta_{mn}$, and $[c]_{mn} = c_{mn}$.

The exchange evolution depends on the detuning δ between the alkali and noble-gas spins, and the coupling is maximal on resonance $\delta = 0$. If the quantum signal is mapped on the uniform mode of the alkali spins at storage, then after a π pulse [with $T' - T \approx \pi/(2J)$], we find the efficiency

$$\eta_{\text{in}}^{(S \rightarrow K)} = \frac{\langle \hat{\mathcal{K}}^\dagger \hat{\mathcal{K}} \rangle_{T'}}{\langle \hat{\mathcal{S}}^\dagger \hat{\mathcal{S}} \rangle_T} = \sum_m |c_{0m}|^2 \exp\left(-\frac{\gamma_m^{(s)} \pi}{2J}\right). \quad (\text{H6})$$

* These authors contributed equally to this work.

[1] A. I. Lvovsky, B. C. Sanders & W. Tittel, *Nature Photon.* 3, 706–714 (2009).

- [2] N. Sangouard, C. Simon, H. De Riedmatten & N. Gisin, *Rev. Mod. Phys.* 83, 33–80 (2011).
- [3] L. M. Duan, M. D. Lukin, J. I. Cirac & P. Zoller, *Nature*, 414, 413–418 (2001).
- [4] M. Aspelmeyer et al., *Science* 301, 621 (2003).
- [5] K. Heshami, D. G. Englanda, P. C. Humphreys, P. J. Bustarda, V. M. Acostac, J. Nunn & B. J. Sussman, *J. Mod. Opt.* 63, 2005–2028 (2016).
- [6] A. Seri, D. Lago-Rivera, A. Lenhard, G. Corrielli, R. Osellame, M. Mazzer, and H. de Riedmatten, *Phys. Rev. Lett.* 123, 080502 (2019).
- [7] Y. Wang, J. Li, S. Zhang, K. Su, Y. Zhou, K. Liao, S. Du, H. Yan & S. Zhu, *Nat. Photonics* 13, 346 (2019).
- [8] M. Zugenmaier, K. B. Dideriksen, A. S. Sørensen, B. Albrecht & E. S. Polzik, *Commun. Phys.* 1, 76 (2018).
- [9] J. L. O'Brien, *Science* 318, 1567–1570 (2007).
- [10] H. J. Kimble, *Nature*, 453, 1023–1030 (2008).
- [11] H. Li, J. Dou, X. Pang, C. Zhang, Z. Yan, T. Yang, J. Gao, J. Li, X. Jin, arXiv preprint arXiv:2002.11759 (2020).
- [12] K. Jensen, W. Wasilewski, H. Krauter, T. Fernholz, B. M. Nielsen, M. Owari, M. B. Plenio, A. Serafini, M. M. Wolf & E. S. Polzik, *Nat. Phys.* 7, 13–16 (2011).
- [13] J. Appel, E. Figueroa, D. Korystov, M. Lobino, and A. I. Lvovsky, *Phys. Rev. Lett.* 100, 093602 (2008).
- [14] V. I. Yudin, A. V. Taichenachev, Y. O. Dudin, V. L. Velichansky, A. S. Zibrov, and S. A. Zibrov, *Phys. Rev. A* 82, 033807 (2010).
- [15] I. K. Komins, *Phys. Rev. Lett.* 100, 073002 (2008).
- [16] J. Kong, R. Jiménez-Martínez, C. Troullinou, V. G. Lucivero, and M. W. Mitchell, *Nat Commun* 11, 2415 (2020).
- [17] K. Hammerer, A. S. Sørensen & E. S. Polzik, *Rev. Mod. Phys.* 82, 1041–1093 (2010).
- [18] I. Novikova, R. Walsworth & Y. Xiao, *Laser Photon. Rev.* 6, 333–353 (2012).
- [19] M. D. Lukin, *Rev. Mod. Phys.* 75, 457 (2003).
- [20] M. Fleischhauer, A. Imamoglu, and J. P. Marangos, *Rev. Mod. Phys.* 77, 633 (2005).
- [21] C. Li, N. Jiang, Y.-K. Wu, W. Chang, Y.-F. Pu, S. Zhang, and L.-M. Duan, *Phys. Rev. Lett.* 124, 240504 (2020).
- [22] J. Guo, X. Feng, P. Yang, Z. Yu, L. Q. Chen, C. Yuan & W. Zhang, *Nat. Commun.* 10, 148 (2019).
- [23] J. Nunn, I. A. Walmsley, M. G. Raymer, K. Surmacz, F. C. Waldermann, Z. Wang, and D. Jaksch, *Phys. Rev. A* 75, 011401(R) (2007).
- [24] D. J. Saunders, J. H. D. Munns, T. F. M. Champion, C. Qiu, K. T. Kaczmarek, E. Poem, P. M. Ledingham, I. A. Walmsley, and J. Nunn, *Phys. Rev. Lett.* 116, 090501 (2016).
- [25] B. Julsgaard, J. Sherson, J. I. Cirac, J. Fiurášek & E. S. Polzik, *Nature* 432, 482–486 (2004).
- [26] C. Schori, B. Julsgaard, J. L. Sørensen, and E. S. Polzik, *Phys. Rev. Lett.* 89, 057903 (2002).
- [27] A. Dantan, N. Treps, A. Bramati, and M. Pinard, *Phys. Rev. Lett.* 94, 050502 (2005).
- [28] M. Hosseini, B. M. Sparkes, G. Campbell, P. K. Lam & B. C. Buchler, *Nat. Commun.* 2, 174 (2011).
- [29] N. Sangouard, C. Simon, M. Afzelius, and N. Gisin, *Phys. Rev. A* 75, 032327 (2007).
- [30] C. T. Nguyen, D. D. Sukachev, M. K. Bhaskar, B. Machielse, D. S. Levonian, E. N. Knall, P. Stroganov, R. Riedinger, H. Park, M. Loncar, and M. D. Lukin, *Phys.*

- Rev. Lett. 123, 183602 (2019).
- [31] G. Heinze, C. Hubrich, and T. Halfmann, *Phys. Rev. Lett.* 111, 033601 (2013).
- [32] D. Serrano, J. Karlsson, A. Fossati, A. Ferrier & P. Goldner, *Nat. Commun.* 9, 2127 (2018).
- [33] D. F. Phillips, A. Fleischhauer, A. Mair, R. L. Walsworth, and M. D. Lukin, *Phys. Rev. Lett.* 86, 783–786 (2001).
- [34] M. D. Eisaman, A. André, F. Massou, M. Fleischhauer, A. S. Zibrov & M. D. Lukin, *Nature*, 438, 837–841 (2005).
- [35] O. Katz & O. Firstenberg, *Nat. Commun.* 9, 2074 (2018).
- [36] M. A. Maynard, F. Bretenaker, and F. Goldfarb, *Phys. Rev. A* 90, 061801(R) (2014).
- [37] E. Distanto, P. Farrera, A. Padrón-Brito, D. Paredes-Barato, G. Heinze & H. de , *Nat. Commun.* 8, 14072 (2017).
- [38] Y. O. Dudin, L. Li, and A. Kuzmich, *Phys. Rev. A* 87, 031801(R) (2013).
- [39] Y. W. Cho, G. T. Campbell, J. L. Everett, J. Bernu, D. B. Higginbottom, M. T. Cao, J. Geng, N. P. Robins, P. K. Lam, and B. C. Buchler, *Optica* 3, 100-107 (2016).
- [40] T. R. Gentile, P. J. Nacher, B. Saam & T. G. Walker, *Rev. Mod. Phys.* 89, 045004 (2017).
- [41] C. Gemmel, et al. *Eur. Phys. J. D* 57, 303 (2010).
- [42] D. M. L. Lilburn, G. E. Pavlovskaya, and T. Meersmann, *J. Magn. Reson.* 229, 173 (2013).
- [43] Couch, M. J. et al. *Mol. Imaging Biol.* 17, 149–162 (2015).
- [44] W. A. Terrano, J. Meinel, N. Sachdeva, T. E. Chupp, S. Degenkolb, P. Fierlinger, F. Kuchler, and J. T. Singh, *Phys. Rev. A* 100, 012502 (2019).
- [45] T. W. Kornack, R. K. Ghosh, and M. V. Romalis, *Phys. Rev. Lett.* 95, 230801 (2005).
- [46] T. G. Walker & M. S. Larsen, *Adv. At. Mol. Opt. Phys.* 65, 373–401 (2016).
- [47] D. A. Thrasher, S. S. Sorensen and T. G. Walker, arXiv preprint arXiv:1912.04991 (2019).
- [48] T. R. Gentile et al. *Physica B (Amsterdam)* 356, 96–102 (2005).
- [49] M. S. Safronova, D. Budker, D. DeMille, D. F. Jackson Kimball, A. Derevianko & C. W. Clark, *Rev. Mod. Phys.* 90, 025008 (2018).
- [50] J. Lee, A. Almasi & M. V. Romalis, *Phys. Rev. Lett.* 120, 161801 (2018).
- [51] F. Allmendinger, W. Heil, S. Karpuk, W. Kilian, A. Scharth, U. Schmidt, A. Schnabel, Yu. Sobolev, and K. Tullney, *Phys. Rev. Lett.* 112, 110801 (2014).
- [52] T. E. Chupp, P. Fierlinger, M. J. Ramsey-Musolf, and J. T. Singh, *Rev. Mod. Phys.* 91, 015001 (2019).
- [53] M. Batz, P. J. Nacher & G. Tastervin, *J. Phys. Conf. Ser.* 294, 012002 (2011).
- [54] T. G. Walker & W. Happer, *Rev. Mod. Phys.* 69, 629 (1997).
- [55] S. Appelt, A. Ben-Amar Baranga, C. J. Erickson, M. V. Romalis, A. R. Young & W. Happer, *Phys. Rev. A* 58, 1412 (1998).
- [56] A. Dantan, G. Reinaudi, A. Sinatra, F. Laloë, E. Giacobino & M. Pinard, *Phys. Rev. Lett.* 95, 123002 (2005).
- [57] O. Katz, R. Shaham & O. Firstenberg, arXiv preprint arXiv:1905.12532 (2019).
- [58] O. Katz, R. Shaham, E. S. Polzik, and O. Firstenberg, *Phys. Rev. Lett.* 124, 043602 (2020).
- [59] O. Katz, E. Reches, R. Shaham, A. V. Gorshkov & O. Firstenberg, arXiv preprint arXiv:2007.08770 (2020).
- [60] W. Happer, Y. Y. Jau & T. Walker. *Optically Pumped Atoms.* 159–218 (WILEY-VCH Press, Germany, 2010).
- [61] A. V. Gorshkov, A. André, M. D. Lukin & A. S. Sørensen, *Phys. Rev. A* 76, 033804 (2007).
- [62] O. Firstenberg, M. Shuker, A. Ron, and N. Davidson, *Rev. Mod. Phys.* 85, 941 (2013).
- [63] R. Shaham, O. Katz, and O. Firstenberg, arXiv preprint arXiv:2006.04243 (2020).
- [64] C. W. Gardiner & P. Zoller, *Quantum Noise* (Springer Verlag, Berlin, 1999), 2nd ed.
- [65] T. Holstein and H. Primakoff, *Phys. Rev.* 58, 1098-1113 (1940).
- [66] A. V. Gorshkov, A. André, M. D. Lukin & A. S. Sørensen., *Phys. Rev. A* 76, 033805 (2007).
- [67] A. V. Gorshkov, A. André, M. Fleischhauer, A. S. Sørensen & M. D. Lukin. *Phys. Rev. Lett.* 98, 123601 (2007).
- [68] A. Dantan and M. Pinard, *Phys. Rev. A* 69, 043810 (2004).
- [69] A. Dantan, A. Bramati, and M. Pinard, *Laser Phys.* 15, 170 (2005).
- [70] A. Dantan, J. Cviklinski, M. Pinard, and Ph. Grangier, *Phys. Rev. A* 73, 032338 (2006).
- [71] A. V. Gorshkov, T. Calarco, M. D. Lukin & A. S. Sørensen, *Phys. Rev. A* 77, 043806 (2008)
- [72] D. E. Rumelhart, G. E. Hinton & R. J. Williams, *Nature* 323, 533–536 (1986).
- [73] N. Qian, *Neural Netw.* 12, 145 (1999).
- [74] J. Sherson, A. S. Sørensen, J. Fiurásek, K. Mølmer & E. S. Polzik. *Phys. Rev. A* 74, 011802(R) (2006).
- [75] C. A. Muschik, K. Hammerer, E. S. Polzik & J. I. Cirac, *Phys. Rev. A* 73 062329 (2006).
- [76] O. Katz, M. Dikopoltsev, O. Peleg, M. Shuker, J. Steinhauer, and N. Katz, *Phys. Rev. Lett.* 110, 263004 (2013).
- [77] G. D. Cates, S. R. Schaefer, and W. Happer, *Phys. Rev. A* 37, 2877 (1988).
- [78] W. Happer, E. Miron, S. Schaefer, D. Schreiber, W. A. van Wijngaarden & X. Zeng. *Phys. Rev. A* 29, 3092–3110 (1984).
- [79] X. Zeng, Z. Wu, T. Call, E. Miron, D. Schreiber & W. Happer. *Phys. Rev. A* 31, 260 (1985).
- [80] M. V. Romalis, *Phys. Rev. Lett.* 105, 243001 (2010).
- [81] M. Auzinsh, D. Budker, and S. M. Rochester *Optically Polarized Atoms* (Oxford University Press, New York, 2010).
- [82] O. Katz & O. Firstenberg, *Commun. Phys.* 2, 58 (2019).
- [83] W. Chalupczak, R. M. Godun, P. Anielski, A. Wojciechowski, S. Pustelny, and W. Gawlik, *Phys. Rev. A* 85, 043402 (2012).
- [84] M. V. Balabas, T. Karaulanov, M. P. Ledbetter & D. Budker, *Phys. Rev. Lett.* 105, 070801 (2010).
- [85] R. Finkelstein, E. Poem, O. Michel, O. Lahad & O. Firstenberg, *Science Advances* 4, 1 (2018).
- [86] F. Ripka, H. Kübler, R. Löw, & T. Pfau, *Science*, 362, 6413, 446-449 (2018).
- [87] K. T. Kaczmarek, P. M. Ledingham, B. Brecht, S. E. Thomas, G. S. Thekkadath, O. Lazo-Arjona, J. H. D. Munns, E. Poem, A. Feizpour, D. J. Saunders, J. Nunn, and I. A. Walmsley, *Phys. Rev. A* 97, 042316 (2018).